Precambrian Research 350 (2020) 105913

Contents lists available at ScienceDirect

Precambrian Research

journal homepage: www.elsevier.com/locate/precamres

# Serra do Barro Branco orthogneiss: An untimely record of West Gondwana amalgamation in the São Roque Domain

Mikaella Balis[a,*], Mario da Costa Campos Neto[b], Adriana Alves[b]

[a] Universidade de São Paulo, Instituto de Geociências, Programa de Pós-Graduação, São Paulo, Brazil
[b] Universidade de São Paulo, Instituto de Geociências, Departamento de Mineralogia e Geotectônica, São Paulo, Brazil

ARTICLE INFO

*Keywords:*
Southern Brasília Orogen
Cryogenian-Ediacaran retroarc magmatism
U-Pb LA-ICP-MS
Sedimentary provenance
Tectonic evolution

ABSTRACT

The Paranapanema-São Francisco convergence is partially recorded in the arc-related high-K calc-alkaline intermediate magmatism of south-eastern Brazil (Southern Brasília Orogen) during the West Gondwana assembly. Similar geochemical affinities are widespread in the crustal fault-bounded slice, São Roque Domain, as in tectonic domains of the eastern São Francisco margin. The São Roque Domain comprises metavolcano-sedimentary sequences of Statherian maximum depositional age. Detrital zircon provenance points to a Rhyacian (2.17 Ga) proximal source belonging to the Paranapanema block. Unprecedented Tonian zircon U-Pb ages suggest a protracted evolution. The domain initiated magmatic activity at 680 Ma (Barro Branco orthogneiss) with weak Hf-Nd radiogenic signatures that agree with the arc evolution of the Socorro-Guaxupé Nappe. Granitoids grading from intermediate metaluminous to evolved peraluminous compositions intruded at 625 Ma (inequigranular orthogneiss) and 620 Ma (Moinho granodiorite). The most voluminous magmatism occurred within 610–590 Ma. Hf-Nd radiogenic compositions of the Ediacaran granitoids imply crustal participation. All granitoids have arc-related affinity with high Sr/Y and LREE, low Nb and Ti, and absence of Eu anomalies that indicate a lower crustal source with residual garnet ( ± amphibole ± rutile). The petrogenetic and geochronological constraints favor a retro-arc setting for the São Roque Domain. Slab roll-back could have led to the northward migration of magmatism (Socorro-Guaxupé Nappe) producing a chronological gap in the retro-arc. The Ediacaran magmatism was probably triggered by the relaxation of the subducting angle. The last-longing subduction beneath the Paranapanema plate might have contributed to the high-K and radiogenic compositions through relamination. Monazite U-Pb ages from 630 to 600 Ma may be evidence of a thermal episode in the retro-arc, overlapping the syn-collisional metamorphism in the Southern Brasília Orogen.

## 1. Introduction

In central-southeast Brazil, the Brasília Orogen is the record of Neoproterozoic plate convergence and collision between three cratonic blocks, São Francisco as the lower plate, Amazonas and Paranapanema and a line of Tonian island arcs (Pimentel, 2016; Fuck et al., 2017; Valeriano, 2017 and references therein) at 670–640 Ma (Piuzana et al., 2003; Reno et al., 2009; Campos Neto et al., 2011; Coelho et al., 2017; Tedeschi et al., 2017). This tectonic process built one of the first continents of Western Gondwana, namely the São Francisco-Paranapanema protocontinent. After 600–580 Ma, the accretion of several terranes southeast of this protocontinent constitutes the NE-trending Ribeira Orogenic System (Heilbron et al., 2017a), which consolidates the West Gondwana margin in the Cambro-Ordovician (Valeriano et al., 2016).

Transition from pre-collisional to late stages of arc evolution is marked by the emplacement of calc-alkaline batholiths and high-K to shoshonitic volcanic rocks (Defant and Drummond, 1990; Tatsumi and Eggins, 1995; Turner et al., 1996; Blatter et al., 2001; Stern, 2002; Putirka and Busby, 2007; Pe-Piper et al., 2009; Ducea et al., 2015). The origin of high-K magmatism is frequently attributed to mantle enriched by previous subductions and triggered by processes such as slab break-off and/or lower crustal delamination. Alternative origins of high-K magmas include low-degree partial melting of “normal” lithosphere (e.g., Stern et al., 1988; Putirka and Busby, 2007; Wang et al., 2017) not exclusively related to late- or post-orogenic stages of continental evolution. High-K calc-alkaline granitoids are widespread in the Socorro-Guaxupé Nappe (magmatic arc domain) and the southern neighbor, São Roque Domain. They are subduction-related with evidence of coeval mafic magmatism (e.g., Haddad, 1995; Ragatky, 1998; Vinagre et al., 2014; Janasi et al., 2016). The metasedimentary record indicates a

* Corresponding author at: Instituto de Geociências – Universidade de São Paulo, Rua do Lago, 562 - Butantã, São Paulo - SP, 05508-080, Brazil.
*E-mail addresses:* mikaella.balis@alumni.usp.br (M. Balis), camposnt@usp.br (M.d.C. Campos Neto), adrianaalves@usp.br (A. Alves).

https://doi.org/10.1016/j.precamres.2020.105913
Received 16 January 2020; Received in revised form 15 August 2020; Accepted 17 August 2020
Available online 27 August 2020

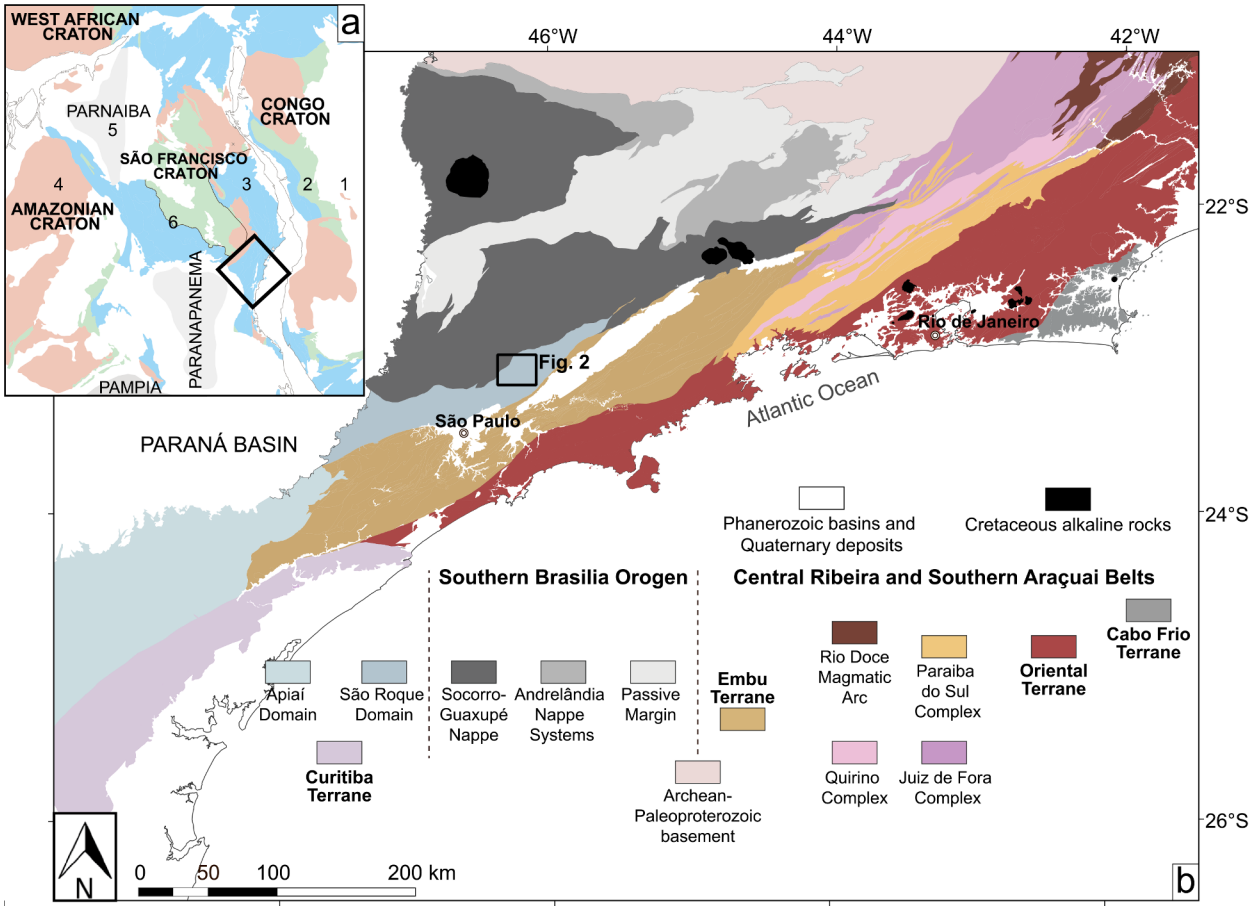


**Fig. 1.** . (a) Tectonic sketch of the reconstruction of Western Gondwana (1- Phanerozoic basins; 2- Proterozoic covers; 3- Neoproterozoic System of Orogens; 4- Basement of the cratons; 5- Covered old blocks; 6-South boundary of São Francisco craton) (Cioffi et al., 2016b). (b) Tectonic map of the orogenic systems that surround the São Francisco craton in south-eastern Brazil (modified from Heilbron et al., 2017a, 2020 and references therein) denoting the studied area (black square).

possible correlation of both domains (Campos Neto, 2000), supported by sedimentary provenance (Henrique-Pinto et al., 2015b).

We present unprecedented data such as bulk-rock geochemistry (elemental and Sm-Nd isotopes) and *in situ* zircon (U-Pb and Hf) and monazite (U-Pb and WDS) determinations. The petrogenesis and geochronology of the São Roque Domain allow the comparison and correlation with other tectonic domains. The paleogeographic scenario gives insight on to whether the São Roque Domain was related to the convergence between the Paranapanema and São Francisco paleoplates.

## 2. Geological setting

The diachronic amalgamation of the West-Gondwana (Fig. 1a) is partly imprinted on the evolution of the Southern Brasília Orogen that was developed during convergence between the Paranapanema (active margin) and São Francisco (passive margin) paleoplates (Brito Neves et al., 1999; Campos Neto, 2000). The Socorro-Guaxupé Nappe (Fig. 1b) is a high-grade, arc-derived terrane of exposed deep Neoproterozoic crust. The magmatic arc remnants are stacked over the passive margin basement (Cioffi et al., 2016a, Cioffi et al., 2016b, Westin et al., 2016), covers (Westin and Campos Neto, 2013; Fumes et al., 2019; Westin et al., 2019; Marimon et al., 2020) and over an allochthonous terrane comprising high-pressure kyanite-bearing granulites, a metasedimentary pile with eclogitic slices and foreland-like metawackes (Andrelândia schists). Such occurrences form a package of flat-lying, east-verging, thick-skinned collisional nappes of *ca.* 640–600 Ma (Campos Neto and Caby, 1999; Trouw et al., 2000; Reno et al., 2009; Campos Neto et al., 2010; Coelho et al., 2017; Tedeschi et al., 2017; Cioffi et al., 2019).

The pre-collisional magmatic arc developed on the active margin of the Paranapanema plate. The arc is divided into three units of Socorro-Guaxupé Nappe, from base to top: (i) enderbitic granulites topped by amphibolite-facies tonalite-granodiorite gneisses; (ii) migmatites that transition to porphyritic granite batholiths, and (iii) garnet ± sillimanite gneisses that grade to peraluminous leucosomes (Campos Neto and Caby, 2000). Charnockite and high-K calc-alkaline suites composed by hornblende-biotite-quartz monzonites-monzogranites with mafic enclaves (Janasi and Ulbrich, 1991; Haddad, 1995; Janasi, 1999; Mora et al., 2014) and subordinate monzodiorites, tonalites, and granodiorites intrude the package. They are partially coeval to a prolonged high to ultra-high temperature metamorphism (up to ~1000 °C) estimated at *ca.* 630–590 Ma (Rocha et al., 2017) or *ca.* 670–590 Ma (Tedeschi et al., 2018).

The Ribeira Belt (Fig. 1b) is a system of orogens extending southwards from the Araçuaí Orogen that comprises a set of independent terranes, each recording an individual tectonic evolution. These were accreted to the southeastern margin of the São Francisco-Paranapanema protocontinent (agglutinated during the Southern Brasília Orogeny) after 580 Ma (Heilbron and Machado, 2003; Heilbron et al., 2017b). The assembly makes up the tectonic scenario of four major terranes – Occidental, Paraíba do Sul-Embu, Oriental, and Cabo Frio (Heilbron et al., 2017a; Corrales et al., 2020). The Paraíba do Sul-Embu Terrane comprises a Cordilleran-type inner-magmatic arc extending from the Araçuaí active margin (Serra da Bolívia-Rio Doce – Corrales et al., 2020; Heilbron et al., 2020). The terrane developed between 650 and 590 Ma with high-grade metamorphic overprinting at *ca.* 580 Ma

(Heilbron et al., 2013; Tedeschi et al., 2016; Novo et al., 2018; Corrales et al., 2020). The Oriental Terrane, also accreted at 580 Ma, shows a succession of slightly juvenile to evolved magmatic arcs built during the Tonian (855–840 Ma), in the Cryogenian-Ediacaran transition (640–620 Ma) and the late-Ediacaran (570–550 Ma – Tupinambá et al., 2000; Fernandes et al., 2015; Peixoto et al., 2017). The terranes unveil the evolution of a long-lived oceanic convergence scenario, ended with an Eo-Cambrian collision – namely Cabo Frio orogeny (Schmitt et al., 2016).

The Araçuaí Orogen occurs at the northern tip of this system and represents a complete orogenic section with passive margin, passive margin-oceanic transition and active margin sequences originated by a frontal collision (580–540 Ma) against the eastern margin of the São Francisco Craton (Pedrosa-Soares et al., 1998; Alkmim et al., 2017; Degler et al., 2017; Peixoto et al., 2018; Amaral et al., 2020).

An alternative hypothesis of intracontinental evolution consists of an extensional regime followed by convergence between the São Francisco-Congo cratons that would drive the Araçuaí-West Congo orogenesis (Fossen et al., 2020) – similar to the alternative Ribeira intracontinental model (Meira et al., 2015). These models, however, do not account for the geochemical and isotopic characteristics of the widespread supra-subduction magmatism described for both orogenic systems.

The Embu Terrane (Fig. 1b) consists of an exotic terrane regarding its tectonic framework (Campos Neto, 2000; Frisch et al., 2011). It is a NE-oriented elongated belt between the São Roque Domain-Socorro-Guaxupé Nappe and the Oriental Terrane, also limited by a shear zone to the north from the Paraiba do Sul Complex (Campos Neto, 2000). The section comprises an Eo-Tonian metasedimentary sequence hosting slightly metaluminous to peraluminous orthogneisses contemporaneous to regional metamorphism (up to upper amphibolite facies and melting) at 800–780 Ma (Cordani et al., 2002; Vlach, 2008; Vinagre et al., 2017; Campanha et al., 2019; Passarelli et al., 2019). This assembly is detached over Paleoproterozoic orthogneisses that hold distinguished chemical and (Nd-Hf) isotopic signatures and lack any record of the Tonian metamorphism (Maurer, 2016; Silva, 2017). The northwestern boundary of the Embu Terrane was masked by the Brasília Orogen collision and later on by late-Ediacaran shear zones, widespread granitic magmatism and metamorphic overprint (Alves et al., 2013, 2016; Silva, 2017; Ribeiro et al., 2019).

### 2.1. São Roque Domain

Two major dextral shear zones delimit the São Roque Domain and are part of the widespread strike-slip system in the eastern margin of the São Francisco craton (Fig. 1b). The Jundiuvira shear zone to the north separates the domain from the Socorro-Guaxupé Nappe, whereas the Buquira-Rio Jaguari-Taxaquara shear zones to the south mark the boundary with the Embu Terrane (Campanha et al., 2019) (Fig. 2a). It comprises two metavolcano-sedimentary sequences with a controversial lithostratigraphy due to complex relations and unconformities: the Serra do Itaberaba Group and São Roque Group *stricto sensu* (Juliani and Beljavskis, 1995 and references therein; Juliani et al., 2000). These sequences were intruded by a voluminous Neoproterozoic magmatism.

#### 2.1.1. Paleoproterozoic (to Mesoproterozoic?) metavolcano-sedimentary sequences

The Serra do Itaberaba Group is a metavolcano-sedimentary sequence that records medium-grade metamorphism (Juliani et al., 1986). It comprises units from base to top that intercalate metamafic, metapelitic, calc-silicate and metavolcanic rocks, and banded iron formations, (Fe-Mg- and Ca-rich) pelites with carbonate lenses, metatuffs, metabasalts and metarhyolites to upper rhythmic schists and a quartzitic unit (Juliani et al., 2000). The basal metapelitic rocks present medium- to high-grade assemblages (garnet, staurolite, kyanite, sillimanite, cordierite, and rarely K-feldspar). The quartzitic unit grades into ( ± biotite)-garnet-sillimanite schists resembling turbidites. A minimum depositional age of *ca.* 1395 ± 10 Ma was obtained from a metandesite above a MORB-like metamafic unit interpreted as an oceanic ridge environment (Juliani, 1993; Juliani et al., 2000 and references therein).

The São Roque Group (Juliani et al., 1986, 2000) comprises a sequence of low-grade rocks represented by feldspathic metarythmites (metawackes) with intercalations of phyllites, slate, metasandstones, metarkoses and metamafic rocks underlain by metaconglomerates and metabreccias (basal units). The southern lithostratigraphy comprises an intermediate unit of low-grade metapelite that extends to the north as an upper unit at the Serra do Itaberaba region (Juliani and Beljavskis, 1995). Deposition was estimated at around ~1.75–1.79 Ga (Van Schmus et al., 1986; Henrique-Pinto et al., 2018) from the age of an interlayered metarhyodacite. Bergmann (1988) interpreted the sequence as a continental rift basin in passive margin, whereas others claim the São Roque Group developed to a Neoproterozoic back-arc basin (e.g., Hackspacher et al., 2000; Juliani et al., 2000).

Zircon provenance studies in the central São Roque Domain advocated for Statherian (~1.75 Ga) and Calymmian (~1.4 Ga) depositional ages, consisting of a lower rift sequence, an intermediate volcano-sedimentary sequence (mainly the Serra do Itaberaba Group) and upper platform turbidites (Henrique-Pinto et al., 2015b). The São Roque Domain quartzites are potentially correlated to the quartzites and schists in the southernmost Socorro-Guaxupé Nappe (Serra do Japi region, Campos Neto, 2000), as shown by the highly similar detrital zircon patterns (Henrique-Pinto et al., 2015b).

#### 2.1.2. Neoproterozoic magmatism

The granitic magmatism of the São Roque Domain is represented by circumscribed plutons and small batholiths often associated with NE-shear zones. The I-type magmatism is typically high-K calc-alkaline with high Sr/Y, Ba and Sr. The main lithotypes vary from porphyritic biotite monzogranites to quartz-monzonites with intermediate composition and predominantly metaluminous character (Janasi and Ulbrich, 1991). The magmatism was potentially generated at deep crustal levels suggested by disequilibrium features observed in plagioclase (Janasi et al., 2016; Lamoso and Janasi, 2019) and coeval mafic magmatism (occurrence of mafic microgranular enclaves). Contamination from the country metasedimentary rocks might have also played a significant role during emplacement. These I-type granitoids were considered to represent syn- to late-collisional emplacements (Campos Neto et al., 1983, 1988; Janasi and Ulbrich, 1991; Ragatky, 1998). There are also subordinate, post-orogenic sub-alkaline occurrences of A-type affinity (Janasi and Ulbrich, 1991). In the central São Roque Domain, the magmatism was constrained within 605–590 Ma, refuting previously reported older ID-TIMS ages believed to carry an inherited component (Janasi et al., 2016 and references therein). Janasi et al. (2016) noted an eastward shift in Hf and Nd isotopes to more radiogenic signatures indicating a progressive contribution of a juvenile component. The isotopic signatures indicate reworking of a 2.4–2.5 Ga-old juvenile protolith and suggest convergence on the eastern margin of the Ribeira Belt (Henrique-Pinto et al., 2015b; Janasi et al., 2016).

Although geological information on the eastern São Roque Domain is scarce, new geochronological data determined that late-orogenic plutons were emplaced within 606–589 Ma (Lamoso and Janasi, 2019) similarly to what is observed in the central region. The Serra do Barro Branco orthogneiss (Fig. 2a) has compositional and structural characteristics of syn-orogenic settings (Campos Neto et al., 1988) with a single U-Pb TIMS age of *ca.* 629 Ma (Ragatky, 1998), thus it represents the oldest occurrence of intrusive rocks in the domain. The Moinho granodiorite is a small intrusion south to the Barro Branco that was dated at *ca.* 620 Ma (SHRIMP U-Pb; Tassinari et al., 2004). Ragatky (1998) argued for reworking of a deep, long-lived crustal source (Nd $T_{DM}$ model ages ~1.7–2.0 Ga) followed by possible juvenile accretions

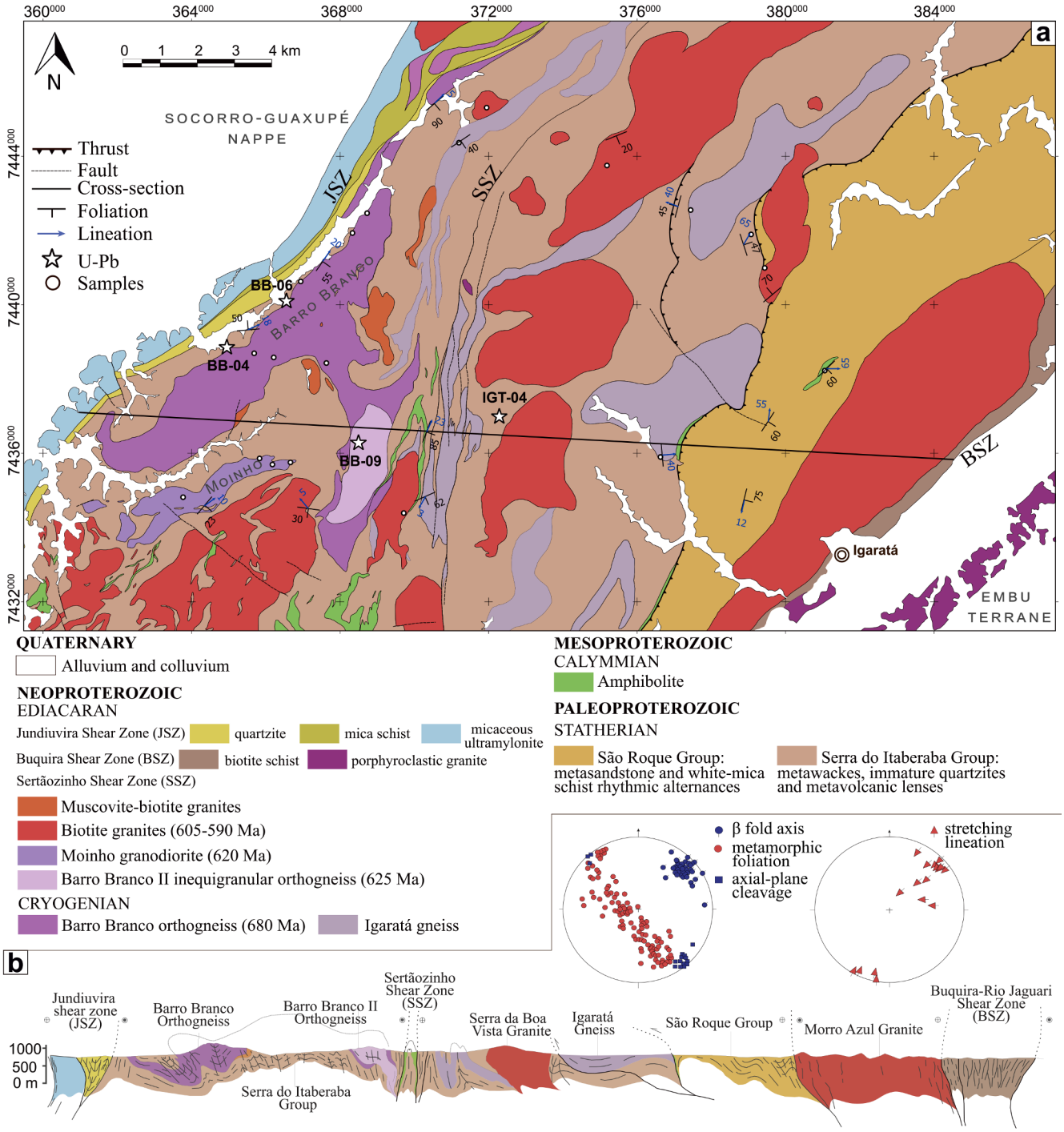


**Fig. 2.** . (a) Detailed geological map of the studied area (modified from Campos Neto et al., 1988). (b) E-W cross-section with stereograms displaying the structural framework.

that marked the late-orogenic magmatism.

## 3. Geology of the granitoid and metavolcano-sedimentary rocks in the eastern São Roque Domain

The targets of this study (Table 1) were heavily sampled (Barro Branco and inequigranular orthogneisses and Moinho granodiorite, Fig. 2a). Other occurrences are represented by single samples and therefore only presented in a descriptive manner. However, a few characteristics were cautiously taken into consideration for interpretation purposes.

The area of study is delimited by two major shear zones (Jundiuvira and Buquira-Rio Jaguari) and intersected by the local Sertãozinho shear zone, that condition the development of mylonitic foliation (Fig. 2a). Sinistral kinematics overprinted by dextral movements (Garcia and Campos Neto, 1997) generated the pervasive $S_2$ foliation observed in the orthogneisses and parallelize the tectonic contacts with country metasedimentary rocks. The foliation gradually shifts from NW to NE that associated with axial-plane cleavages with gently NE-plunging fold axes characterize a cylindrical W-verging fold (Fig. 2b). The stretching lineation defined by feldspar porphyroclasts marks the reorientation of the fold axes supporting a ductile top-to-SW shear zone regime.

**Table 1**
. Data summary.

| Sample | Coordinates | Rock | Unit | Zircon age ± 2σ (Ma) | Monazite age ± 2σ (Ma) | Detrital peak (Ga) | Dating Technique | εNdt | Average εHft ± 2σ | Hf (mean) & Nd $T_{DM}$ (Ga) | References |
|---|---|---|---|---|---|---|---|---|---|---|---|
| BB-04C | 7438847/364952 | Monzogranitic orthogneiss | Barro Branco | 680 ± 4 | | | LA-ICP-MS U-Pb | | −4.6 ± 1.4 | 1.88 | This study |
| BB-09 | 7436272/368498 | Monzogranitic orthogneiss | Barro Branco II | 625 ± 7 | | | LA-ICP-MS U-Pb | | −11.7 ± 1.6 | 2.29 | This study |
| BB-44A | 7434814/363772 | Monzogranite | Moinho | | | | | −12.90 | | 1.96 | This study |
| BB-31C | 7444362/371202 | Monzogranitic orthogneiss | Igaratá[+] | | | | | −7.21 | | 1.62 | This study |
| IGT-04C | 7436981/372290 | Bt gneiss | Serra do Itaberaba Group | 593 ± 3 | | | LA-ICP-MS U-Pb | −11.61 | | 1.76 | This study |
| BB-06 | 7440090/366557 | Ms-Bt schist | Serra do Itaberaba Group | | | 2.173 | LA-ICP-MS U-Pb | | +1.8 ± 1.5 | 2.78 | This study |
| IGT-04D | 7436981/372290 | Bt paragneiss | Serra do Itaberaba Group | | 600 ± 2 | 2.171 | LA-ICP-MS U-Pb | −0.86 | | 2.47 | This study |
| 8 | * | Monzogranitc to granodioritic orthogneiss | Barro Branco II | 629 ± 11 | | | TIMS U-Pb | −11.55 | | 1.79 | [1] |
| 6 | * | Monzogranitc to granodioritic orthogneiss | Barro Branco II | | | | | −11.72 | | 1.75 | [1] |
| 12 | * | Monzogranite to granodiorite | Moinho | | | | | −11.18 | | 1.88 | [1] |
| SP-02 | * | Granodiorite | Moinho | 620 ± 11 | | | SHRIMP U-Pb | −13.24 | | 2.09 | [2] |
| CT13J | * | Granodiorite | Moinho | | | | | −14.49 | | 2.13 | [2] |

[1] Ragatky (1998).
[2] Tassinari et al. (2004).
*References do not provide sample coordinates; localizations are marked in map figures.
[+] Literature considers the Igaratá gneisses synchronous to the Barro Branco (Campos Neto et al., 1988; Tassinari, 1988). The Igaratá samples are, thus, presented within the geochemical data array of the Barro Branco orthogneiss.

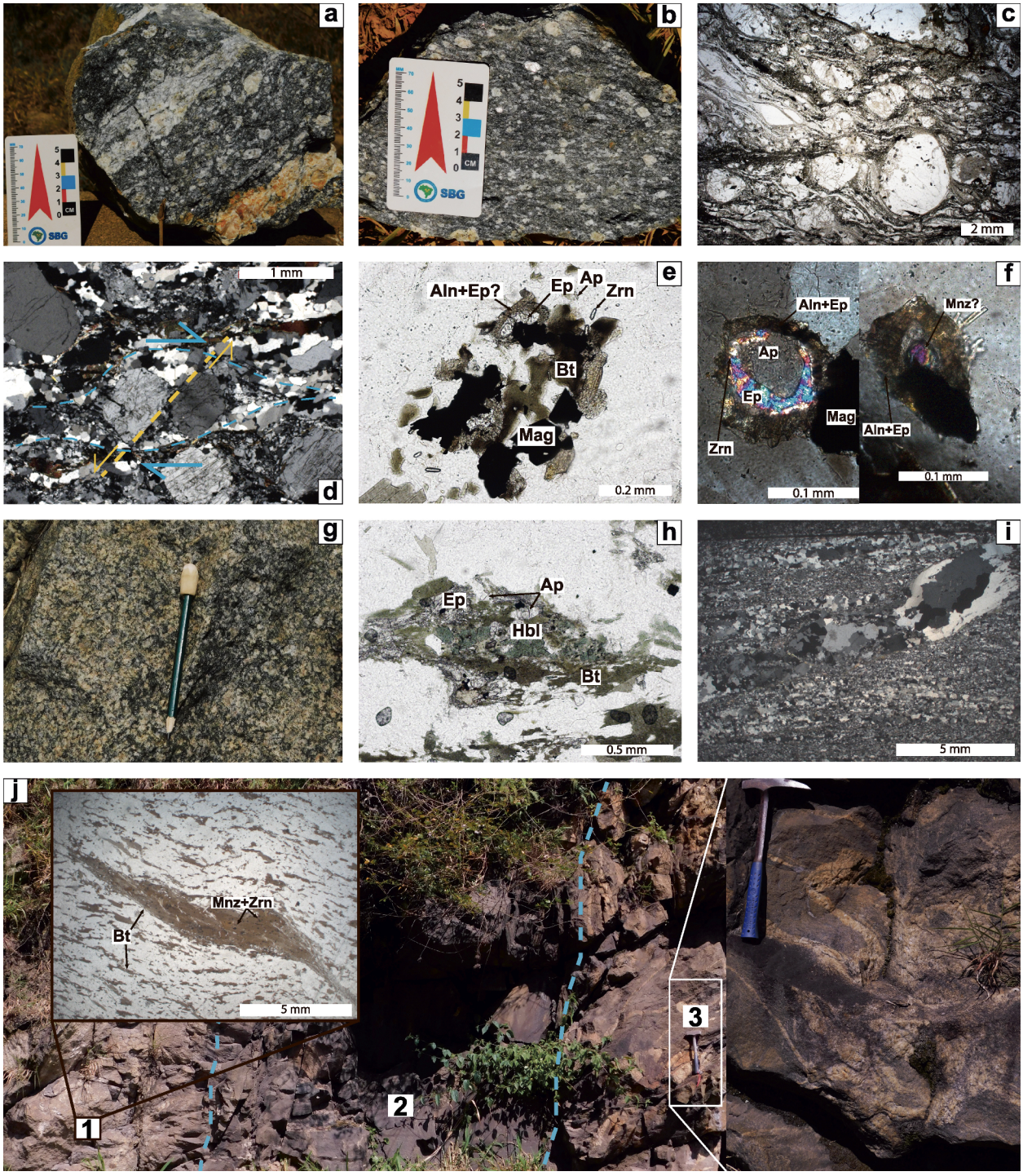


**Fig. 3.** . Macro- and micro-scale petrography of the area of study. Mineral abbreviations after Siivola and Schmid (2007). (a–d) The Barro Branco biotite orthogneiss displays a protomylonitic foliation with S-C fabric and distinctive compositional layering. Greenish biotite enfolds feldspathic porphyroclasts (c) and antithetic fractures (d). (e–f) The Barro Branco II inequigranular orthogneiss presents remarkable, complex coronal textures involving allanite, epidote, zircon and/or monazite, commonly associated with plagioclase, magnetite and biotite. Phase relations within the coronas vary either with apatite/epidote or monazite nuclei (f). (g, h) The Moinho granodiorite exhibits subtle foliation and a coarse-grained porphyritic fabric with biotite and hornblende as main mafic phases. Apatite is abundant and often related to epidote surrounding biotite + hornblende. (i) Sample IGT-04C is represented by a grey, fine-grained biotite gneiss that is cut by oblique, discontinuous granitic structures resembling clasts. (j) Outcrop IGT-04 presents complex relations between several rocks: (1) fine-grained biotite paragneiss (sample IGT-04D) with micaceous S-C lenses hosting numerous inclusions of zircon and monazite; (2) a mafic, tonalitic gneiss composed of biotite-rich (IGT-04H) and hornblende-rich (IGT-04E) layers; (3) a deformed quartz + feldspar + biotite granitoid (not sampled) displaying compositional layers, with fold interference and axial plane-foliation, also marked by extensional features in the hinge.

### 3.1. Serra do Barro Branco orthogneiss

The Barro Branco orthogneiss (Fig. 2) is one of the largest intrusions represented by a folded body alongside smaller sheet. This gneiss has porphyroblastic texture (up to 2 cm) with a fine-grained inequigranular matrix (≤1 mm) that evolves to a protomylonitic foliation near the shear zones (Fig. 3a-b). Composition varies from tonalite to granodiorite and monzogranite (quartz + plagioclase + K-feldspar) with biotite as the main mafic phase (Supplementary Material SM-1). Accessory minerals are titanite, allanite, apatite, epidote, magnetite, zircon and -rarely- monazite. The greenish biotite marks the $S_2$ foliation, concentrated in lepidoblastic bands (Fig. 3c). High-temperature ductile features (such as "fish"-, δ- and σ-) on feldspar porphyroclasts transition to brittle antithetic fractures with recrystallized biotite and quartz strain shadows (Fig. 3d). In the granoblastic bands, quartz ribbons with interlobate boundaries indicate grain boundary migration. Titanite-free samples have reddish biotite and form coronal associations of epidote + allanite + apatite.

### 3.2. Barro Branco II: inequigranular orthogneiss

The unit is composed by an inequigranular (0.4–1.6 mm) occurrence (sampled as the main Barro Branco in Ragatky, 1998) of a biotite orthogneiss (Fig. 2). It is a monzogranite (quartz + plagioclase + K-feldspar) with biotite as the main mafic phase and accessory phases such as allanite, apatite, zircon, and monazite. The biotite has reddish color (similar to titanite-free Barro Branco samples) and marks the $S_2$-foliation. The orthogneiss comprises remarkable coronal textures formed by allanite + epidote + apatite (Fig. 3e–f). Although phase relations are complex, hybrid zones of allanite + epidote fine aggregates are ubiquitous. In few cases, we observe monazite and/or zircon in the core of coronas. Such textures have been linked to the break-down of primary monazite (e.g., Broska and Siman, 1998; Finger et al., 1998; Ondrejka et al., 2012). Given secondary muscovite and chlorite occurrences are low-temperature (post-magmatic) associations, monazite break-down was probably induced by fluid activity in the shear zones (e.g., Vlach, 2008).

### 3.3. Moinho granodiorite

The Moinho Granite outcrops to the south of the Barro Branco (Fig. 2a) as a small intrusion of (hornblende)-biotite granodiorite with porphyritic texture intertwined by a subtle foliation (Fig. 3g). The foliation is marked by a greenish biotite ± hornblende moulding feldspar (microcline and plagioclase) and flame perthite phenocrysts (≤1 cm) (Fig. 3h). The inequigranular matrix (0.4–1.8 mm) is composed of interlobate quartz + plagioclase + microcline (and perthites) with granophyric texture. Grain boundaries are filled with recrystallized quartz and feldspar sub-grains. Accessory phases are titanite, abundant apatite, allanite, magnetite, epidote, and zircon.

### 3.4. Metavolcaniclastic rock

A fine-grained biotite gneiss (IGT-04C) composed of a quartz + plagioclase + K-feldspar matrix is intertwined by biotite crystals that mark the foliation. Accessory phases are magnetite, apatite, allanite and zircon. The gneiss is cut by coarse-grained granitic, discontinuous lenses with trace occurrences of white mica (sericite?) and carbonate that resemble a granitic clast (Fig. 3i). Based on the petrographic characterization and zircon grain pattern (further detailed), we suggest the sample consists of a metavolcaniclastic rock.

### 3.5. Metasedimentary rocks

In this study, we analyzed two samples from the metasedimentary sequence: a biotite schist (BB-06) and a biotite paragneiss (IGT-04D). The biotite schist was sampled between the Barro Branco orthogneiss and the Jundiuvira shear zone (Fig. 2a). The rock alternates thick lepidoblastic bands of biotite + muscovite with thin quartz ribbons. The foliation molds "fish" feldspar grains, forming an S-C fabric. The biotite paragneiss was sampled in the central region, close to the Sertãozinho shear zone (Fig. 2a). The paragneiss is composed of a fine-grained quartz + feldspar matrix with oriented biotite. Coarse-grained mica fish lenses (biotite + secondary muscovite) are common with numerous inclusions of monazite and zircon (Fig. 3j-1). Monazite grains from this sample were analyzed for mineral chemistry (WDS-EPMA) and U-Pb dating (LA-ICP-MS). Metasedimentary outcrops displayed numerous leucogranitic and quartzitic veins.

### 3.6. Mafic gneiss

The hornblende-biotite gneiss was sampled at the IGT-04 site along the metavolcaniclastic rock and biotite paragneiss (Fig. 3j-2). It consists of a mafic gneiss that obliquely intersects the metavolcaniclastic rock and is associated with a granitoid rock (not sampled, Fig. 3j-3). The gneiss presents distinct portions of either hornblende-rich or biotite-rich (IGT-04H) layers that alternate thin tonalitic bands with titanite and apatite as important accessory phases. Only sample IGT-04H was used for whole-rock chemistry.

### 3.7. Igaratá gneisses

The Igaratá gneisses are scattered elongated bodies of biotite gneisses that resemble the inequigranular orthogneiss. They occur mostly between the Sertãozinho and Buquira shear zones (Fig. 2). The foliation is more subtle and marked by a reddish biotite. These gneisses are monzogranites with inequigranular matrix, locally with plagioclase and K-feldspar porphyroblasts. Substitution of biotite by chlorite and sericitization of feldspars are common. Accessory minerals are titanite, metamict allanite, epidote, zircon, and apatite.

### 3.8. Biotite granites

The biotite granites are small circumscribed plutons (Fig. 2) with phaneritic inequigranular texture, sometimes with subtle foliation. The composition is predominantly monzogranitic with biotite as the main mafic phase. Accessory phases are titanite, allanite, epidote, apatite, magnetite, and zircon. Quartz displays undulose extinction and has interlobate contacts with microcline and plagioclase. Chlorite often replaces biotite.

## 4. Analytical methods

### 4.1. U-Th-Pb geochronology of zircon and monazite

Zircon (from five samples) and monazite grains (from one sample) were prepared and mounted in epoxy for LA-ICP-MS U-Pb dating at the Centro de Pesquisas Geocronológicas (IGc-USP) following the routine of Sato et al. (2008). Given two out of five zircon samples were metasedimentary rocks, the grains were randomly handpicked to avoid biased age peaks. Imaging techniques included cathodoluminescence (CL) for zircon and back-scatter electron (BSE) for monazite grains via scanning electron microscopy (SEM).

LA-ICP-MS analyses used a 193ηm Excimer laser (Photon Machines) coupled to a Thermo-Neptune multicollector ICP-MS with 6 mJ energy at a repetition rate of 6–7 Hz. The laser spot was set to 25 μm for monazite and 32 μm for zircon with 40–60 s ablation per spot. The He carrier gas transported the ablated material (0.7 L/min) into the ICP-MS. The MC-ICP-MS was set to mixed cup configuration at a 1100 W radiofrequency power, refrigeration Ar flux rate of 15 L/min, auxiliary Ar flux rate of 0.7 L/min and sample gas flux of 0.6 L/min. Elemental and downhole fractionations were corrected combining measurements

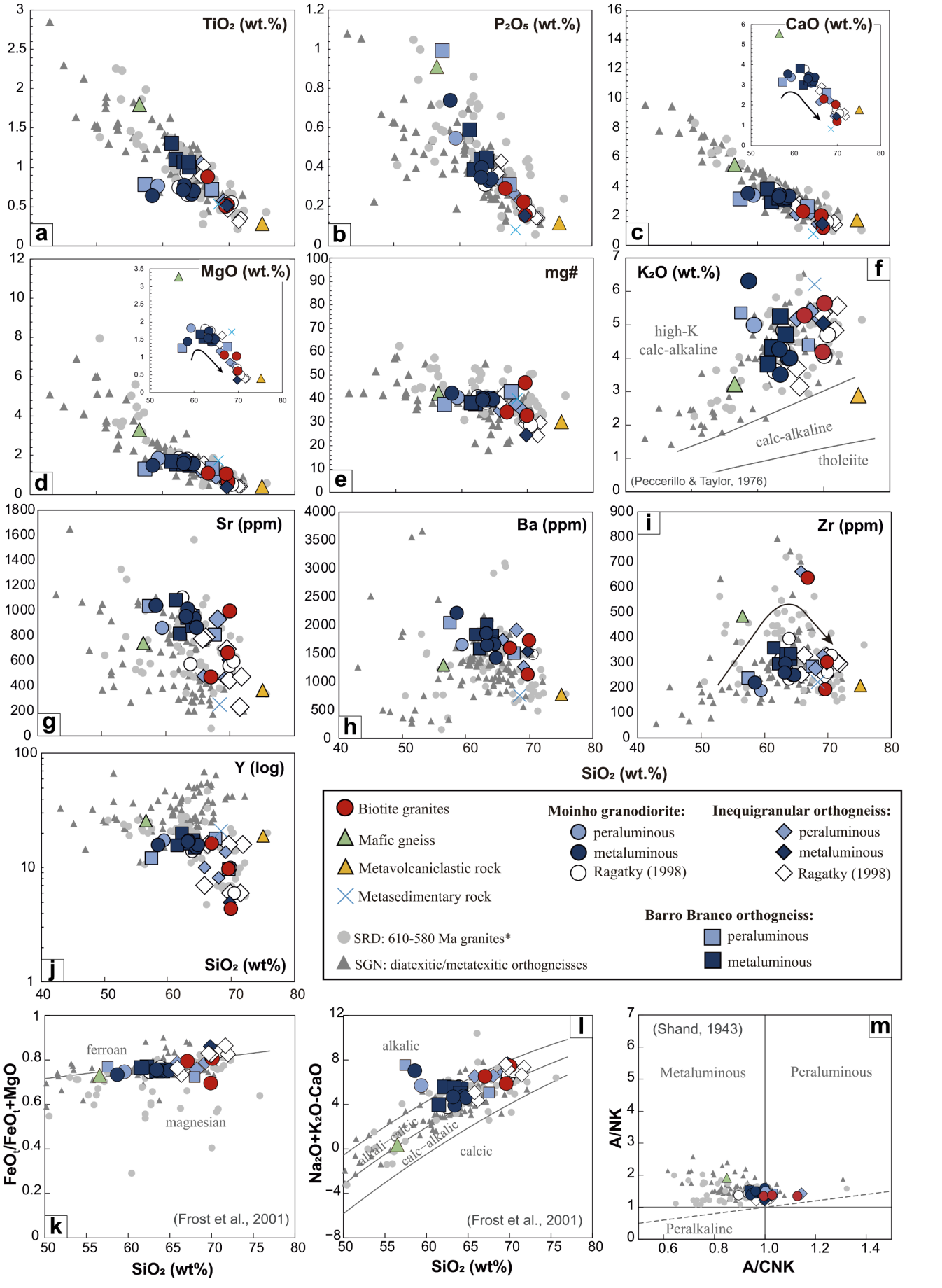


*(caption on next page)*

**Fig. 4.** . (a–j) Harker plots with relevant major, minor elements, and mg# of all sampled rocks. (f, k–m) Granitoid classification schemes (Shand, 1943; Peccerillo and Taylor, 1976; Frost et al., 2001). Grey symbols represent data from literature: (i) SRD: 610–580 Ma granites (Ragatky, 1998; Janasi et al., 2016; Lamoso and Janasi, 2019) and granitoids from the eastern domain (Campos Neto et al., 1988; Ragatky, 1998); (ii) SGN: hbl-bt orthogneisses (Janasi, 1999), Pinhal-Ipuiuna batholith (Haddad, 1995), Serra da Água Limpa batholith (Vinagre et al., 2014), Pinhal and São José do Rio Pardo diatexites, granulites and metatexites (Mora et al., 2014) and metatexitic orthogneisses (Gengo, 2014).

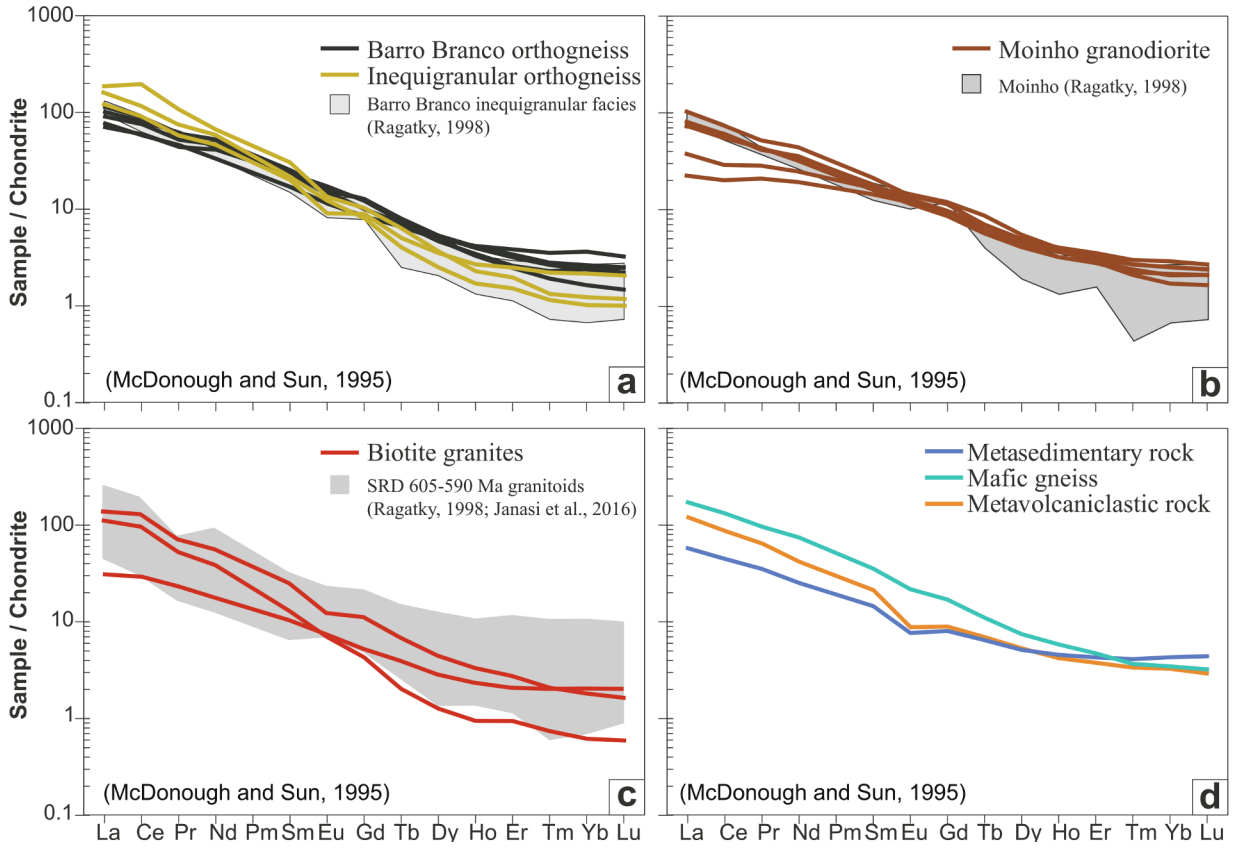


**Fig. 5.** . Chondrite-normalized (McDonough and Sun, 1995) REE fractionation patterns of all samples. Fields represent São Roque Domain data from literature (Ragatky, 1998; Janasi et al., 2016).

of blank, NIST-612 (Woodhead and Hergt, 2001), standard GJ-1 (Elhlou et al., 2006) or Monazite-44069 (Aleinikoff et al., 2006) and unknowns. Initial $^{204}$Pb was corrected according to Stacey and Kramers (1975). Data reduction was peformed with in-house software (Siqueira et al., 2014) and treated with Isoplot (Ludwig, 2003) and IsoplotR (Vermeesch, 2018). The provenance study also relied on the Arizona LaserChron spreadsheets. We filtered the data using common Pb ≤ 10%, CL zircon textures, weighted average plots to separate potential populations and inherences, and 100 ± 10% of concordance for $^{206}$Pb/$^{238}$U dates (< 1 Ga) and $^{206}$Pb/$^{207}$Pb dates (> 1 Ga, provenance).

### 4.2. Whole-rock and trace-element geochemistry

Whole-rock compositional analyses were performed at NAP-Geoanalítica (IGc-USP). Major element compositions of twenty-four samples were obtained by X-ray fluorescence spectrometry with a Phillips-PW2400 XRF spectrometer. Sample preparation followed the routine described in Mori et al. (1999). Quality control relied on duplicates and reference standards JB-1a and JG-1a. Trace elements, including REE, were measured for twenty-one samples with a Perkin Elmer ICP-MS ELAN 6100 DRC after the procedures described in Navarro et al. (2008). Quality control relied on JG-3 and JR-1 reference materials. Geochemical plots and spidergrams were produced using Excel and GCDKit software (Janoušek et al., 2006).

### 4.3. Isotope geochemistry

#### 4.3.1. Whole-rock Sm-Nd isotopes

Neodymium isotope determinations for four samples were held at CPGeo facility (IGc-USP) with a Thermo-Neptune ICP-MS. Sample preparation involved total dissolution in HF and $HNO_3$ until complete evaporation in Paar bombs at 200 °C, followed by 6 N HCl washes and overnight evaporation. The isotopes of interest were retrieved using ion-exchange columns following the procedures described in Sato et al. (1995).

$^{143}$Nd/$^{144}$Nd isotopic ratios were normalized to $^{146}$Nd/$^{144}$Nd = 0.7219 (DePaolo, 1981) and the average JNDi-1 standard of $^{143}$Nd/$^{144}$Nd = 0.512103 (average laboratory value of the last twelve months). The $\varepsilon Nd_{(0)}$ units were calculated after $[(^{143}Nd/^{144}Nd)_{sample}/0.512638] - 1$ (Hamilton et al., 1983).

#### 4.3.2. Lu-Hf in zircon

Hafnium isotope determinations for three samples were performed at the CPGeo facility (IGc-USP) via LA-ICP-MS. The analyses were acquired under the same conditions of those employed for the U-Pb data except for the laser spot (47 μm), a He flux rate of 0.25 L/min plus a $N_2$ flux rate of 1.2 mL/min to reduce oxide formation in the plasma. Cup configuration in the multicollector was set to L4 = $^{171}$Yb, L3 = $^{173}$Yb, L2 = $^{174}$Hf, L1 = $^{175}$Lu, C = $^{176}$Hf + $^{176}$Lu + $^{176}$Yb, H1 = $^{177}$Hf, H2 = $^{178}$Hf, H3 = $^{179}$Hf and H4 = $^{181}$Ta. The analytical routine involved measurements of blank, GJ1-82C standards (Elhlou et al., 2006)

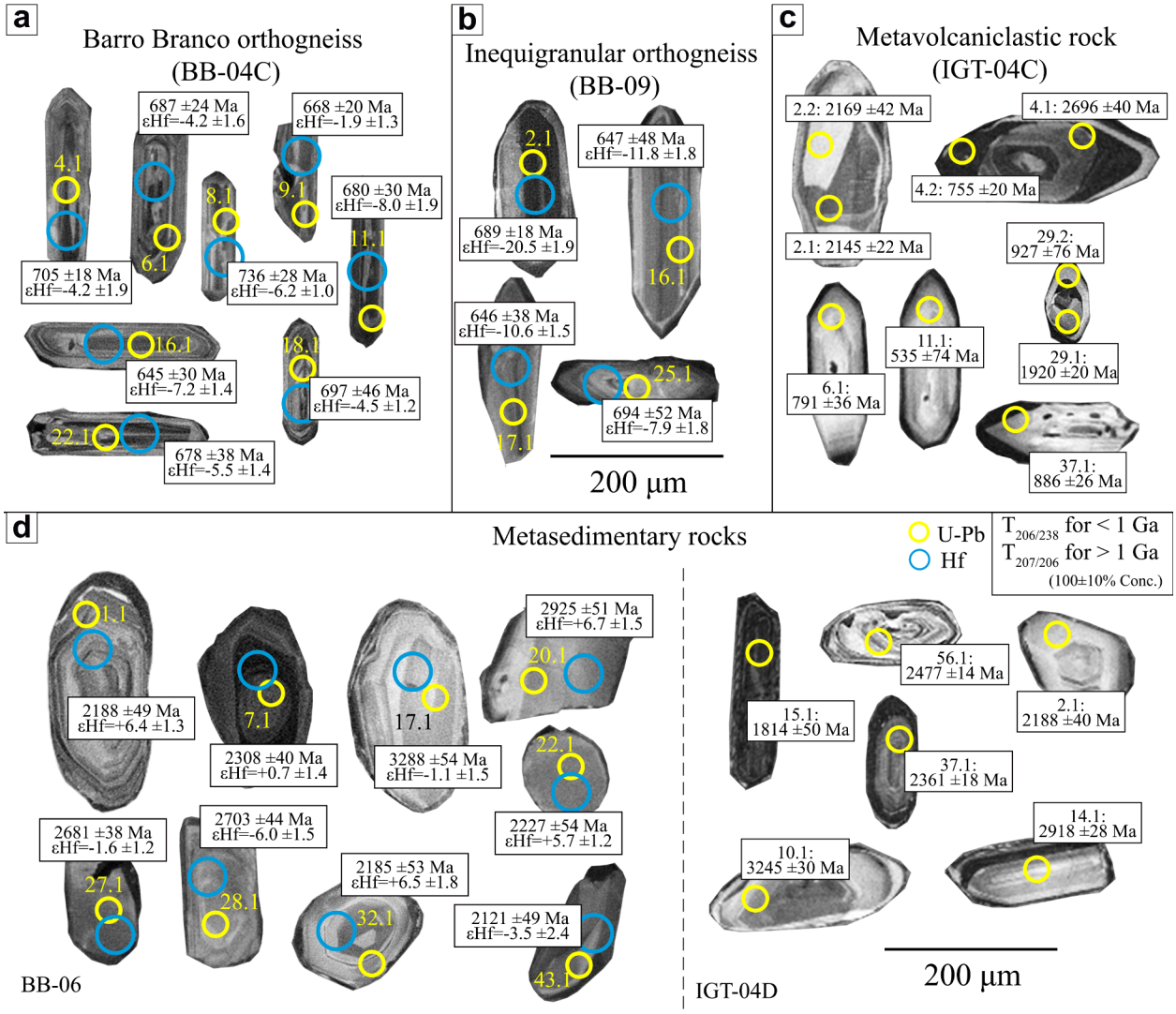


**Fig. 6.** . Cathodoluminescence images of representative zircon grains from granitoid samples (a) BB-04 and (b) BB-09), (c) the metavolcaniclastic rock (IGT-04C), and (d) metasedimentary rocks (samples BB-06 and IGT-04D). Images display U-Pb and Hf spot analyses.

and mud tank. Data reduction was made with in-house spreadsheet using $^{176}Lu$ decay constant = $1.867e^{-11}$ (Söderlund et al., 2004), present-day $^{176}Hf/^{177}Hf$ = 0.28325 (DM) and 0.282785 (CHUR) and $^{176}Lu/^{177}Hf$ = 0.0384 (DM) and 0.0336 (CHUR) (Griffin et al., 2002; Bouvier et al., 2008). For subtraction of the interference of $^{176}Yb$ and $^{176}Lu$ over $^{176}Hf$, we considered the following relative abundance ratios: $^{173}Yb/^{176}Yb$ = 0.7938128 (Chu et al., 2002) and $^{176}Lu/^{175}Lu$ = 0.02656 (Blichert-Toft et al., 1997). Mass bias corrections were calculated considering $^{173}Yb/^{171}Yb$ = 1.130172 (Segal et al., 2003) and $^{179}Hf/^{177}Hf$ = 0.7325 (Patchett and Tatsumoto, 1980). For εHft calculations, 't' refers to single age U-Pb analyses or the crystallization age of the rocks for discordant grains.

### 4.4. EPMA-monazite chemistry

Wavelength-dispersive spectrometry analyses (WDS) of monazite grains were held at the NAP Geoanalítica (IGc-USP) using a JEOL JXA-8530F Field Emission Electron Probe Microanalyzer (FE-EPMA). Calibration conditions were 20 kV and a 50 nA current with a 5 µm diameter beam. The applied standards were natural minerals (fluorapatite, albite, diopside, hornblende, fayalite, wollastonite, microcline, zircon, ilmenite, rutile), REE (and Y)-phosphates (Sm, Gd, Dy, Yb, La, Ce, Pr, Nd) and oxides (Sr, Ba, Th, U).

## 5. Results

### 5.1. Whole-rock geochemistry

Whole-rock compositions are enlisted in SM-2. Geochemical data of granitoids, orthogneisses and migmatites from the São Roque Domain and Socorro-Guaxupé Nappe were compiled for comparison. The data array defines a linear differentiation trend along with the literature compilation. All samples describe negative correlation of $TiO_2$, $Fe_2O_{3(t)}$, MgO, CaO, $Al_2O_3$ and $P_2O_5$ towards the evolved members while $K_2O$ contents increase with silica (Fig. 4a–f). Rocks with granitic composition are products of a high-K calc-alkaline magmatism with intermediate 57–70% $SiO_2$ and 3.5–6.3% $K_2O$, straddling along the metaluminous-peraluminous boundary. The granitoids are magnesian to slightly ferroan and predominantly alkali-calcic (Frost et al., 2001) (Fig. 4k–m).

The Barro Branco orthogneiss presents the most scattered data and range from primitive to evolved $SiO_2$ compositions (57–68%). The primitive end overlaps the Moinho granodiorite samples (59–65%) whereas evolved samples match the behavior of the inequigranular orthogneiss (66–70%) and biotite granites (67–70%). In terms of $TiO_2$, the Moinho granodiorite detaches from the trend due to significantly lower contents. The CaO, $Fe_2O_{3(t)}$ and MgO plots describe inflections at

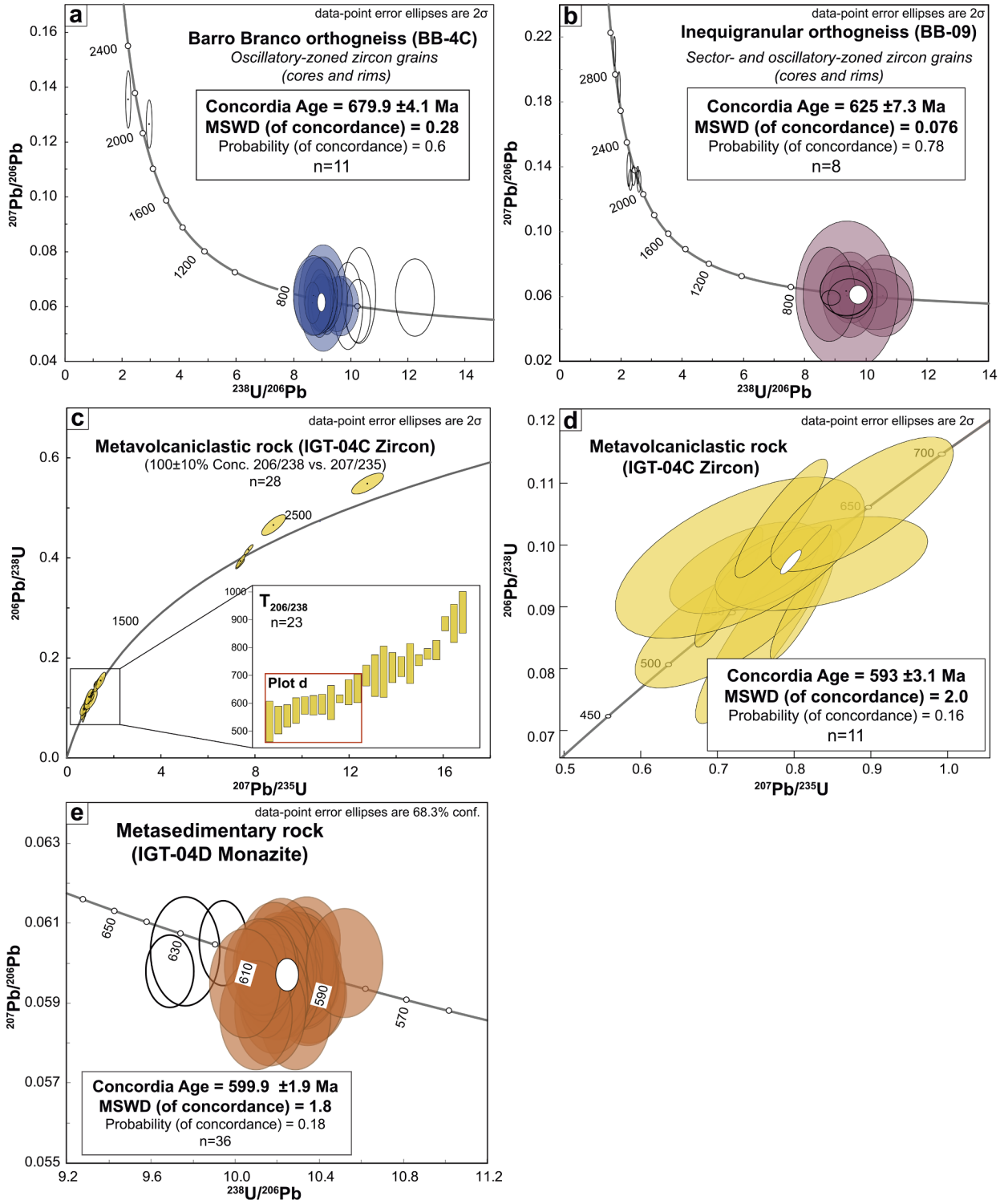


**Fig. 7.** . (a,b) Tera-Wasserburg Concordia plots of the Barro Branco and inequigranular orthogneiss. (c) Wetherill plot displaying the broad age spectra of the metavolcaniclastic rock with detail on the Neoproterozoic populations (weighted average distribution). (d) Wetherill Concordia age of the youngest Neoproterozoic zircon population. (e) Tera Wasserburg Concordia age of monazite from the biotite paragneiss, further discussed in item 5.4.

approximately 60% $SiO_2$ (Fig. 4c-d) whereas $Al_2O_3$ and $P_2O_5$ mark a shift from strongly to moderately negative slopes (Fig. 4b). The Mg# number is virtually uniform (37–43) (Fig. 4e). Likewise, the MgO contents vary within a narrow range of 0.4–1.8% (Fig. 4d). The granitoids have high Ba (1308–2210 ppm) and Sr, the latter more enriched in the Barro Branco orthogneiss (809–1079 ppm) and Moinho granodiorite (858–1032 ppm) (Fig. 4g–h). All samples have low Zr contents (190–665 ppm) and reached saturation around ~62% $SiO_2$ (Fig. 4i). Low Y contents (4–26 ppm) are another relevant feature, with few considerably low values in the evolved samples (e.g., inequigranular orthogneiss and biotite granites) (Fig. 4j). Therefore, such signatures produce high Sr/Y ratios (as further discussed).

Chondrite-normalized (McDonough and Sun, 1995) REE fractionation patterns (Fig. 5a–d) have overall slight negative slopes with near-

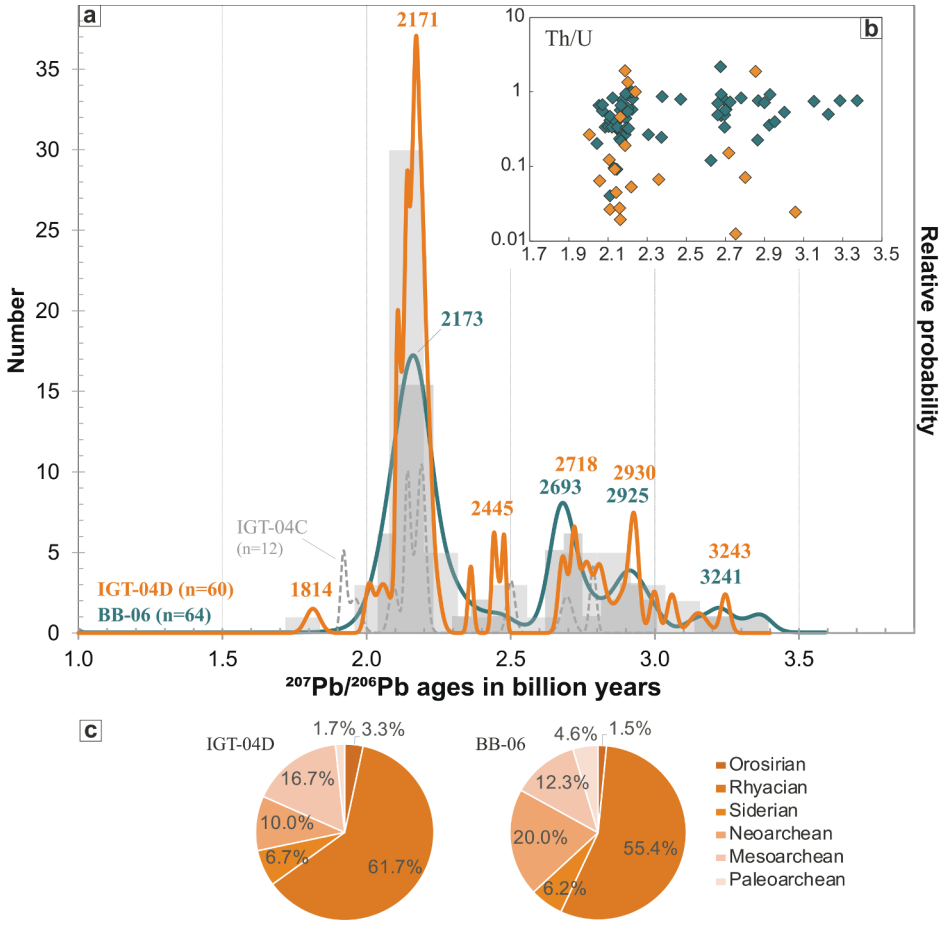


**Fig. 8.** . (a) Probability density curves of the detrital zircon dataset from two metasedimentary rocks (samples BB-06 and IGT-04D) along with the inherences from the metavolcaniclastic rock (sample IGT-04C – grey dashed curve) for virtual comparison, with peak $^{207}Pb/^{206}Pb$ ages and respective (b) Th/U ratios. (c) Pie charts describe the zircon population percentages from each period.

flat HREE and absent-to-weakly-negative Eu anomalies. Unlike the Barro Branco orthogneiss and Moinho granodiorite, the evolved granitoids show pronounced anomalies (Eu/Eu* ~0.7) (Fig. 5a,c). They are also more enriched in LREE and depleted in HREE, thus, resulting in variably stronger REE fractionation slopes [(La/Lu)N = 15–189]. Our data did not reproduce Gd and Tm anomalies described in Ragatky (1998) for Moinho samples, implying possible analytical issues (Fig. 5b).

The mafic gneiss and metavolcaniclastic rock define the least and most evolved end-members of the dataset and were classified as andesite-trachyandesite and rhyolite, respectively (Middlemost, 1994). The mafic gneiss presented exceptionally high MgO (3.3%), Nb (36 ppm), V (123 ppm) and Y (26 ppm). Conversely, the metasedimentary rock is depleted in $P_2O_5$ (0.08%), CaO (0.8%) and Sr (246 ppm) while enriched in Rb (279 ppm). The metavolcaniclastic and metasedimentary rocks present the most pronounced Eu anomalies, the latter forming a slight concave-up HREE pattern (Fig. 5d).

### 5.2. Zircon typology, U-Pb ages and Hf isotopes

#### 5.2.1. Barro Branco orthogneiss

Zircon crystals from sample BB-04C are 100–300 μm long and prismatic. We identified two major zircon populations: (i) fine-scale oscillatory zoned crystals, with aspect ratios up to 4:1 and (ii) sector zoning and elongate prisms (up to 6:1). CL images show all zircon grains have dark narrow rims and exhibit locally resorbed and recrystallized domains (Fig. 6a). In addition, two sub-rounded (2:1) oscillatory-zoned zircon grains with relict old cores were observed. Twenty-three grains were analyzed for LA-ICP-MS U-Pb (see Supplementary Material SM-3). Th/U ratios range 0.3–2.7 and show no correlation with age nor texture/shape. Discordant grains (n = 8), inheritances (n = 2), and two outliers were rejected from the Concordia age calculation (hollow ellipses). The $^{206}Pb/^{238}U$ dates (n = 11) yielded a Concordia age of *ca.* 680 ± 4 Ma (MSWD = 0.28) interpreted as the crystallization time of the protolith (Fig. 7a).

*In situ* Hf analyses (n = 10, Supplementary Material SM-4) yielded ε values from −8 (1.9) to + 0.9 (0.7) and $^{176}Lu/^{177}Hf$ ratios of 0.0004–0.0019. Although Hf spots were placed in the same textural context of U-Pb sites, whenever possible, signatures do not form a strict correlation with time. The positive and weakly radiogenic ε values imply an older juvenile component. Regardless of zoning styles, both clear cores and oscillatory zoned rims show restricted Hf interval (0.282129–0.282381) leading to the hypothesis that the 80–100 Ma difference observed in such crystals represents the crystallization timespan of the protolith.

#### 5.2.2. Inequigranular orthogneiss

Zircon crystals from sample BB-09 are 100–250 μm long and CL images reveal a vast variety of textures. The main zircon populations are (i) elongated crystals (aspect ratios from 3:1 to 5:1) with weak oscillatory and sector zoning, (ii) medium-CL homogeneous crystals and (iii) crystals with aspect ratios from 1:1 to 2:1 and oscillatory zoning revealed to represent old inherences (Fig. 6b). Dark narrow rims are ubiquitous and more pronounced in weakly zoned and homogeneous crystals. Twenty-six grains were analyzed for LA-ICP-MS U-Pb (SM-3). The $^{206}Pb/^{238}U$ concordant single analyses range from 694 to 584 Ma and yield a Concordia age of *ca.* 625 ± 7 Ma (n = 8; MSWD = 0.077; Fig. 7b) interpreted to represent the crystallization age of this rock. Rejected data (hollow ellipses) consist of discordant and inherited grains, and a *ca.* 689 Ma-old antecryst (in the sense of Miller et al., 2007).

*In situ* Hf analyses (n = 10, SM-4) yielded εHft = −12.9 (2.1) to

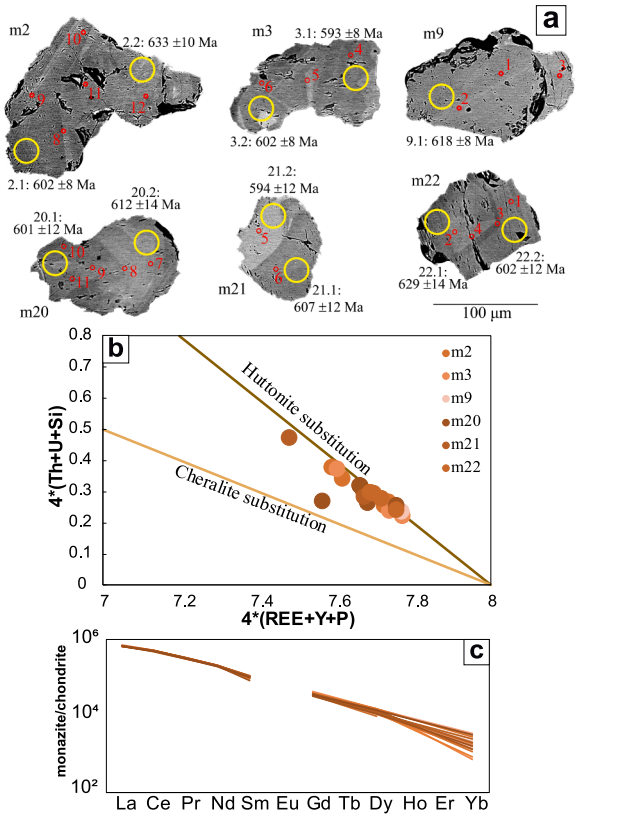


**Fig. 9.** . (a) BSE images of six monazite grains with U-Pb age spots (LA-ICP-MS) and WDS chemical profiles. (b) Cheralite and huttonite substitution vectors of the monazite grains. (c) Chondrite-normalized (McDonough and Sun, 1995) REE fractionation patterns of monazite.

−7.9 (1.8) that only overlap the most radiogenic values of the Barro Branco. $^{176}Hf/^{177}Hf(t)$ (0.282024–0.282140) and $^{176}Lu/^{177}Hf$ (0.00008–0.0005) ratios correlate with ages, although seven ε values were based on the crystallization age of this rock. The Hf signature of the antecryst is an outlier (εHf = −21.9 and 0.281772).

#### 5.2.3. Metavolcaniclastic rock

Sample IGT-04C comprises a complex set of zircon populations (Fig. 6c). Forty-eight spots were analyzed for LA-ICP-MS U-Pb (SM-3). The 800–500 Ma group includes 80–200 µm long crystals that are bright-CL homogeneous to weakly (oscillatory and sector) zoned with aspect ratios from 4:1 to 5:1 and Th/U of 0.2–2.8. Dark oscillatory-zoned crystals often overgrow bright relict (Paleoproterozoic to Archean) cores. There is a significant number of fragments and dark narrow rims in CL images. Two grains present dark, U-rich overgrowths dated at 755 Ma and 777 Ma. Based on age ( ± error) distribution diagrams (Fig. 7c), we separated a group of $^{206}Pb/^{238}U$ single analyses within 535–652 Ma that yielded a Concordia age of *ca.* 593 ± 3 Ma (MSWD = 2, acceptable for n = 11; Spencer et al., 2016 – Fig. 7e). Single ages around 700 Ma (n = 9) fall off the Tera-Wasserburg Concordia field describing a slightly reverse discordance. Along with an isolated group of ~900 Ma single ages (n = 3), the broad age spectrum is inconclusive.

#### 5.2.4. Metasedimentary rocks

Detrital zircon grains from two samples were analyzed for LA-ICP-MS U-Pb. Sample BB-06 comprises three populations (Fig. 6d). Grains with aspect ratios up to 2:1 are 150–340 µm long with weak sector and oscillatory zoning that overgrow relict cores. Fragments are smaller (130–170 µm long) with flow textures. Rounded, homogeneous dark grains (1:1) are 100–150 µm long. Grains from sample IGT-04D are 140–300 µm long with aspect ratios 2:1–3:1. A zircon population comprises weak oscillatory zoning, dark to medium luminescence and relict cores. Other grains are weakly sector-zoned with bright luminescence and one grain is oval (~1:1). All crystals present dark overgrowths of 20–50 µm. None of the samples showed a clear correlation between shape/texture and age. Probability density plots (Fig. 8a) of the $^{207}Pb/^{206}Pb$ dates highlight a main Rhyacian peak of *ca.* 2.17 Ga (55–62%) and two minor peaks of *ca.* 2.7 Ga (10–20%) and *ca.* 2.9 Ga (12–17%) (Fig. 8c). Sample IGT-04D also marked a minor peak at *ca.* 2.45 Ga. The youngest detrital zircon dates *ca.* 1.81 Ga. The density curve of the metavolcaniclastic rock is used for comparison and mirrors the main detrital peaks.

Sample BB-06 was targeted for *in situ* Hf analyses (n = 20). The dataset comprises strongly positive and negative values of εHft from −6 (1.5) to +7.2 (1.6). The zircon population of 2.1–2.4 Ga has $^{176}Lu/^{177}Hf$ ratios ranging from 0.00028 to 0.00136, similar to the > 2.5 Ga-old population (0.0007 to 0.0014).

### 5.3. Nd isotopes

Four samples were analyzed for whole-rock Sm-Nd isotopes (Supplementary Material SM-5). The εNd(t) was calculated based on the obtained crystallization U-Pb ages and the *ca.* 620 Ma (SHRIMP U-Pb) zircon age of the Moinho granodiorite (Tassinari et al., 2004). Depleted mantle model ages (Nd $T_{DM}$) were calculated after DePaolo (1981). A biotite orthogneiss sampled as Barro Branco (BB-31C) presented $^{147}Sm/^{144}Nd$ = 0.100300 and $^{143}Nd/^{144}Nd$ = 0.511840, yielding the least radiogenic $\varepsilon Nd_{680}$ (−7.2) and $T_{DM}$ of 1.62 Ga. The Moinho granodiorite (BB-44A) presented similar $^{147}Sm/^{144}Nd$ (0.100500) and lower $^{143}Nd/^{144}Nd$ (0.511586) yielding more radiogenic $\varepsilon Nd_{620}$ (−12.9) and $T_{DM}$ of 1.96 Ga. The metavolcaniclastic rock (IGT-04C) yielded lower $^{147}Sm/^{144}Nd$ ratio (0.091671). For this sample, we obtained $\varepsilon Nd_{593}$ of −11.6, and $T_{DM}$ of 1.76 Ga. The metasedimentary rock (IGT-04D) presented high $^{147}Sm/^{144}Nd$ (0.107129). The εNd(t) was determined for the Rhyacian detrital peak ($\varepsilon Nd_{2.17\ Ga}$ = −0.9) and the youngest detrital zircon ($\varepsilon Nd_{1.81\ Ga}$ = −5) with model age of 2.47 Ga. We also recalculated the Nd data for samples labelled as Barro Branco and Moinho by Ragatky (1998). The Barro Branco samples in fact correspond to the inequigranular orthogneiss and yielded $\varepsilon Nd_{625}$ = −11.6/−11.7 and $T_{DM}$ 1.75–1.79 Ga. Note that the inequigranular orthogneiss, Moinho granodiorite and metavolcaniclastic rock have radiogenic crustal signatures.

### 5.4. Monazite composition and U-Th-Pb age

Sample IGT-04D provided a monazite-rich fraction of sub-rounded and fractured grains 50–175 µm long. BSE images showed that the dominant texture is a subtle patchy zoning (nearly homogeneous) with bright to medium response. Sector- and weak concentric zoning occur to a lesser extent (Fig. 9a). Thirty-nine grains were analyzed for LA-ICP-MS U-Pb (Supplementary Material SM-3). The $^{206}Pb/^{238}U$ dates are uniform within uncertainties and yield a Concordia age of *ca.* 600 ± 2 Ma (n = 36; MSWD = 1.8) (Fig. 7e). Three zoned monazite grains yielded older dates (618, 629 and 633 Ma).

Six grains were analyzed for chemical composition (WDS-EPMA, Supplementary Material SM-6). The WDS spots were placed both adjacent to U-Pb spots and throughout the crystals (Fig. 9a). The monazite composition is typically Ce-rich, with chemical variations mainly controlled by the huttonite exchange $Th^{4+} + Si^{4+} = REE^{3+} + P^{5+}$ (Linthout, 2007; Fig. 9b) producing high Th contents (2.8–6.7 wt%). Bright BSE domains respond to Th composition reaching up to 0.071 apfu. Chondrite-normalized (McDonough and Sun, 1995) REE patterns are uniform, strongly enriched in LREE and steadily decrease towards HREE with significant variations of Yb (Fig. 9c). The concentric zoning relates to chemical variations, thus allowing to distinguish cores and rims. Rims tend to be enriched in HREE + Th + Y and depleted in

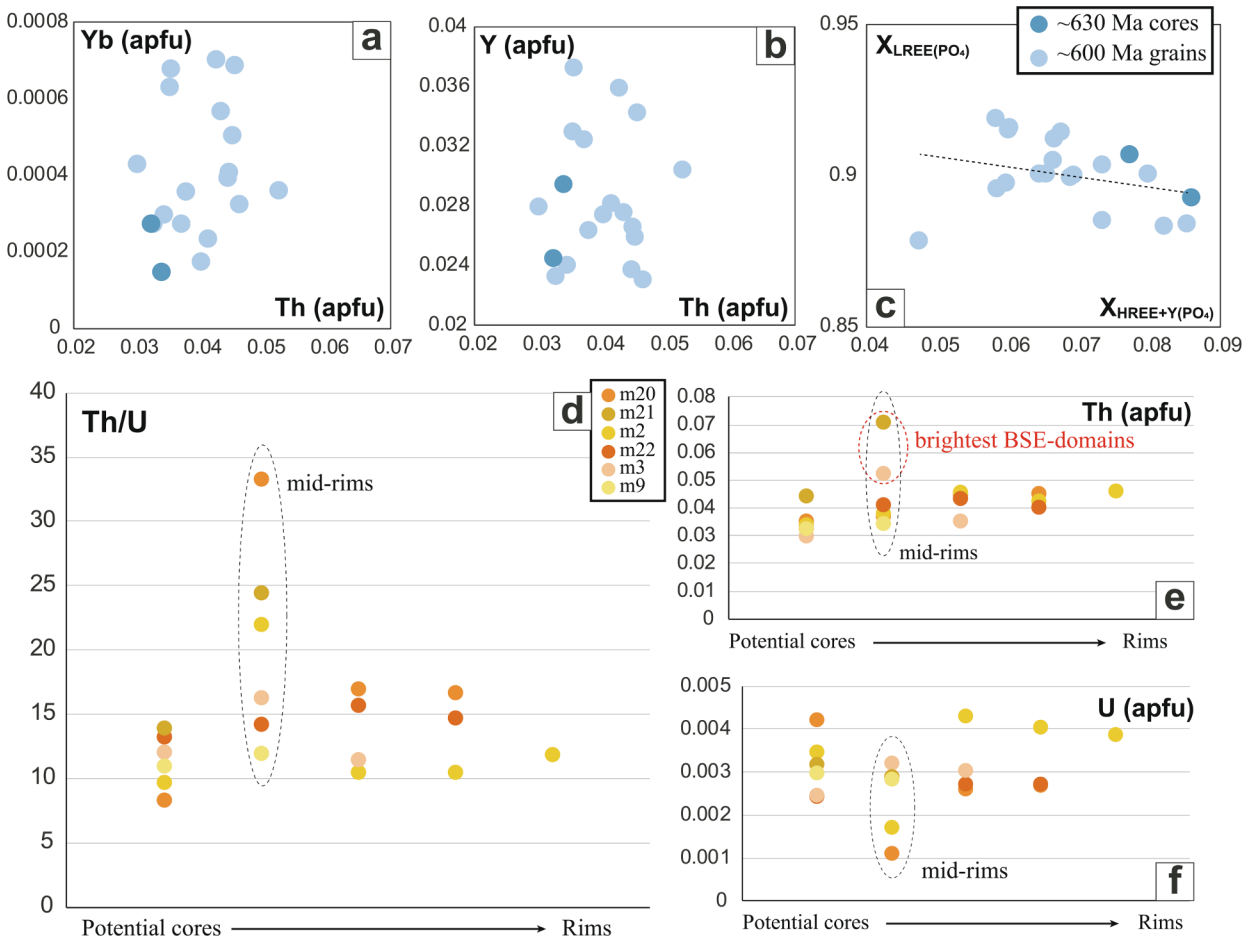


**Fig. 10.** . (a–c) WDS monazite chemical plots vs. age. Molar fractions were calculated according to Pyle et al. (2001). (d–f) Chemical monazite profiles. Spot positions are not in scale, they solely illustrate variations from cores to rims.

LREE compared to cores (Fig. 10a–c). Monazite grains m2 and m22 show relevant intra-grain U-Pb age differences considering uncertainties. Both grains have cores of *ca.* 630 Ma with low Yb + Th and high LREE whereas the outermost domains date *ca.* 602 Ma with opposite chemical signatures.

We observed that the inferred cores have lower Th/U ratios (8.4–14, Fig. 10d–f). Intermediate regions between cores and rims (namely mid-rims) show anomalous increase of Th/U (12–33) due to seemingly independent peaks of Th and troughs of U. This mid-rim pattern could either correspond to resorption zones in the crystals or hold a geological meaning.

## 6. Discussion

### 6.1. Petrogenesis of the granitoid rocks

The Barro Branco is remarkable in that it records a protracted zircon U-Pb history from Tonian to Cryogenian ages (ca. 680 Ma). The inequigranular facies describes a time-constrained differentiation trend, since chemically evolved, peraluminous rocks span a long crystallization period from Tonian to Ediacaran (ca. 625 Ma). Granitoids in the domain describe a joint evolution of high-K calc-alkaline affinity (e.g., Janasi et al., 2016; Lamoso and Janasi, 2019).

Magmas derived from lower crustal sources hold key signatures recognized in the magmatism of the São Roque Domain (Ragatky, 1998; Janasi et al., 2016; Lamoso and Janasi, 2019). Garnet-rich ( ± clinopyroxene ± rutile) and plagioclase-poor sources are known to produce high-Sr intermediate magmas with flattened HREE patterns, low Y, and lack of negative Eu anomalies (Moyen, 2009) (Fig. 11a,b). The granitoids presented in this study (particularly the Barro Branco orthogneiss and Moinho granodiorite) describe a high-K calc-alkaline intermediate magmatism with high Sr/Y (30–220), LILE enrichment and low Ti-Nb (Fig. 11b). Discrete Eu anomalies (Eu/Eu*) define a subtle fractionating trend with $SiO_2$ (slightly pronounced in the inequigranular orthogneiss and biotite granites), which indicates that plagioclase was not ubiquitous in the source (Fig. 12a). Although Dy/Yb *versus* $SiO_2$ characterize fractionation of amphibole (Davidson et al., 2007), it is unlikely amphibole would alter trace elements in such scale (Fig. 12b). It is possible garnet was overprinted by amphibole during crystallization (Moyen, 2009). Residual rutile (and/or amphibole) at higher pressures (e.g., Tang et al., 2019) could produce the Nb anomalies and low $TiO_2$ compositions of these rocks. Lower crustal assemblages also involve abundant apatite (compared to zircon) that generate high-Th/La melts (Plank, 2005 and references therein). The early apatite saturation ($P_2O_5$-$SiO_2$) at 940–1060 °C (Harrison and Watson, 1984) might represent the *liquidus*. The apatite saturation temperatures and Zr undersaturation further suggest a deep-seated parental source.

In Fig. 12c, we observe the studied rocks replicate the formation of felsic crust during the Archean (Chiaradia, 2015). Magmatism potentially derived from the melting of mafic rocks at high pressures and differentiation of the rising melts through thick crust helped develop the calc-alkaline trend, anchored on positive correlation between Sr/Y and La/Yb (Chiaradia, 2015; Profeta et al., 2015; Fig. 12d). The variable LILE and LREE enrichment coupled to negative Nb-Ti anomalies are diagnostic of subduction-related magmas (Tatsumi and Eggins,

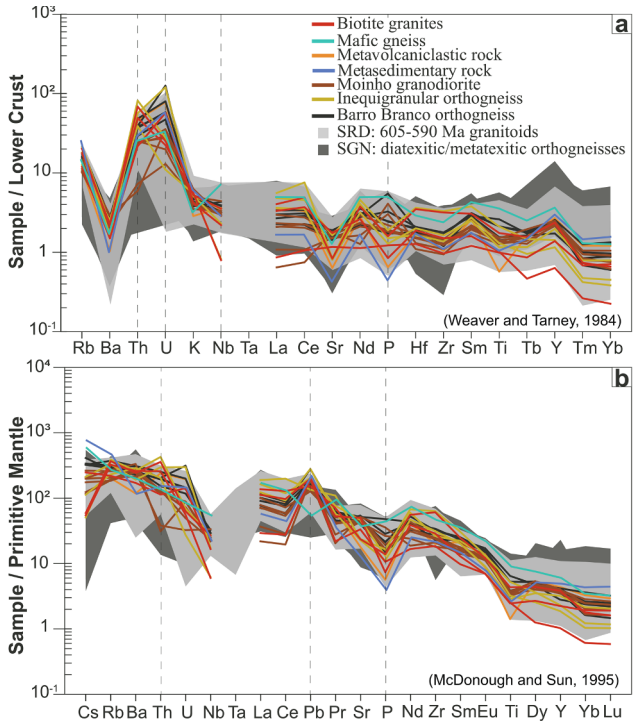


**Fig. 11.** . (a) Trace-elemental fractionation patterns normalized to the lower crust (Weaver and Tarney, 1984) and (b) primitive mantle (McDonough and Sun, 1995).

1995 and references therein).

Considering the subduction-related deep origin of magmatism, Hf-Nd isotopes provided insights on the petrogenetic evolution through geological time. Hf in zircon yielded a wider spectrum of depleted mantle model ages ($T_{DM}$). $T_{DM}$ model ages indicate a crustal reservoir extracted somewhere between 1.6 and 2.1 Ga (Fig. 13a,b). The 680 Ma-old Barro Branco shows weak radiogenic signatures implying a juvenile component. The εHf reveals an isotopic progression from the Barro Branco to the evolved inequigranular orthogneiss (Fig. 13b,c). The inequigranular orthogneiss (ca. 625 Ma) and Moinho granodiorite (ca. 620 Ma; Tassinari et al., 2004) were concomitantly emplaced hosting stronger radiogenic signatures, though bulk-rock compositions diverge. They potentially originated from mixed sources given the older Hf $T_{DM}$ model ages (2.1–2.3 Ga) that overlap the isotopic data of the metasedimentary rocks (Fig. 13a,b). These rocks probably experienced crustal contamination during emplacement and/or a crustal addition to the source.

### 6.2. Insights from zircon provenance

We briefly approach the detrital zircon provenance of the eastern São Roque Domain. Two samples are under-representative of the studied area; thus, we combined our data with provenance studies of the central São Roque Domain (Henrique-Pinto et al., 2015a,b). We used the Kolmogorov-Smirnoff (K-S) test and cumulative distribution (CDF) to analyze the data (Fig. 14). The K-S test showed that most P-values are > 0.05 (95% confidence level). The samples from this study present a high correlation (P = 0.529). Regarding the data compilation, sample BB-06 (close to the Jundiuvira shear zone) highly correlates with PJ-1 M (P = 0.815) and JP-01 (P = 0.690) whereas sample IGT-04D (center of the studied area) highly correlates with JP-19 (P = 0.721) and JP-01 (P = 0.287). The studied samples are less likely associated with VT-03 and VT-04. However, a few P-values are > 0.05 and, thus, we cannot discard the possibility of contribution (in part) from a common source.

We conclude the eastern São Roque Domain more likely shared a parent source with the southern region of the Socorro-Guaxupé Nappe (Serra do Japi) and south region of the studied area. (Pico do Jaraguá and Serra do Pirucaia). The metasedimentary rocks are *metawackes* that indicate sediment immaturity by the presence of detrital K-feldspar and plagioclase. The Hf-Nd isotopes suggest a juvenile accretion between 2.3 and 2.5 Ga that preceded the Rhyacian peak (*ca.* 2.17 Ga) (Fig. 13b). These features altogether imply a paleogeographic proximity of the São Roque Domain to the source.

### 6.3. Metamorphism

The Serra do Itaberaba Group hosts medium-grade metamorphic rocks (Juliani et al., 2000) and, in the eastern section, it records conditions of biotite zone with development of a regional foliation. Metamorphic age determinations are scarce and obtained from U-rich overgrowths on detrital zircon, dated at 584 ± 47 Ma (LA-ICP-MS U-Pb) (Henrique-Pinto et al., 2015b).

Monazite grains that grew on the foliation of a metasedimentary rock revealed BSE textures of metamorphic monazite. U-Pb dating estimated a crystallization age at *ca.* 600 Ma and two oscillatory-zoned grains with cores of *ca.* 630 Ma. Th concentrations vary 3–7% within the interval of magmatic and hydrothermal monazite (Catlos, 2013 and references therein). The Th range is partly reflected on anomalous Th/U ratios in the mid-rims that could relate to simultaneous growth of metamorphic zircon (e.g, Rubatto et al., 2006). Two U-rich zircon rims around 750 Ma are the oldest records of a possibly former thermal event.

Metamorphic monazite is believed to have formed under the same conditions responsible for the development of the coronal textures in the inequigranular orthogneiss (e.g., Finger et al., 1998; Vlach, 2008). The host rock consists of a biotite paragneiss with low Ca lacking allanite, a widespread accessory in the granitoids. Spear and Pyle (2010) stated that low-Ca metapelitic rocks grow new monazite from allanite dissolution (e.g., Corrie and Kohn, 2008; Catlos, 2013 and references therein) during prograde metamorphism.

### 6.4. Regional implications

A key aspect of this work is to attribute a significance to the ~680 magmatism (namely the Barro Branco orthogneiss) that became prominent during 610–590 Ma (Janasi et al., 2016; Lamoso and Janasi, 2019) and resolve the tectonic setting of the São Roque Domain. The magmatism interestingly owns characteristics of subduction-related arc activity found in neighbor terranes, such as the high-K calc-alkaline affinity, high LILE and LREE, and low HREE, Nb and Y (Tatsumi and Eggins, 1995; Ducea et al., 2015). High-K, Ba-Sr granitoids related to arc magmatism are widespread in the Southern Brasília Orogen whereas arc-related rocks in the eastern margin of the São Francisco Craton record medium-K high Ba-Sr magmatism (Araçuaí and Ribeira Belts – Corrales et al., 2020). The Socorro-Guaxupé Nappe records a protracted history of arc magmatism initiated at 800–700 Ma, north in the Southern Brasilia Orogen (Tedeschi et al., 2018) that might overlap the metamorphic stage. Some studies attribute older zircon ages to xenocrystic cores defining a main 670–640 Ma pre-collisional stage (Ebert et al., 1996; Hackspacher et al., 2003; Vinagre et al., 2014; Rocha et al., 2018). Isotopic (zircon and bulk-rock) signatures consistent with initiation of subduction show the contribution from an enriched mantle. On a counterpart, arc-related plutonic rocks of the Paraíba do Sul-Embu Terrane of the Ribeira Belt encompass Tonian zircon ages (Corrales et al., 2020) that might represent inherences since crystallization ages around the Barro Branco intrusion (680 Ma) are absent.

#### 6.4.1. Source areas and tectonic setting

The zircon provenance of the São Roque Domain supports a linked

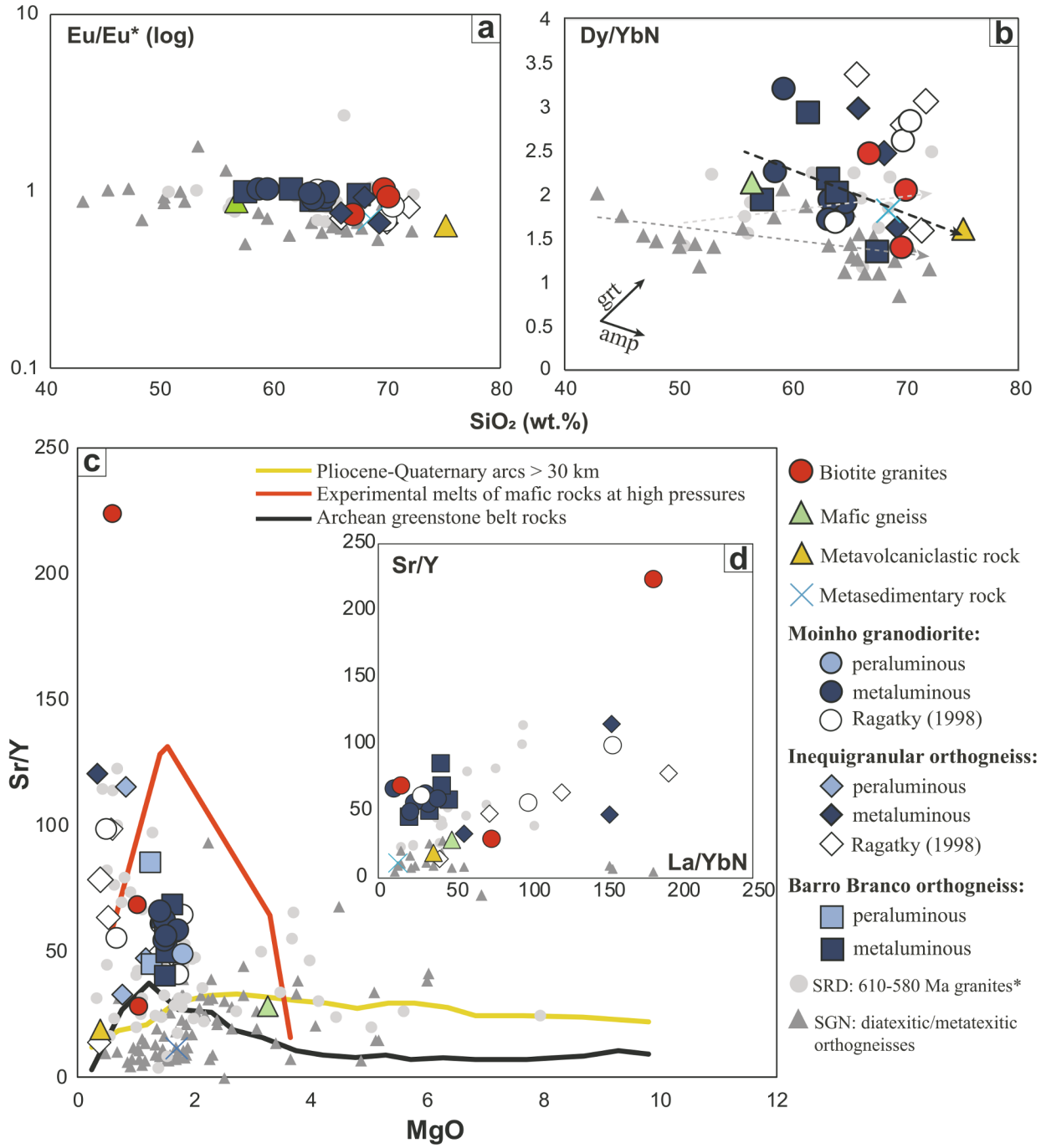


**Fig. 12.** . (a, b) REE chondrite-normalized (McDonough and Sun, 1995) ratios of all samples. In plot (b), garnet and amphibole fractionation patterns were extracted from Davidson et al. (2007). Black dashed arrow reflects all sampled rocks and grey ones represent compiled data from the São Roque Domain (light grey) and Socorro-Guaxupé Nappe (dark grey). (c) MgO vs. Sr/Y of all sampled rocks. Curves were extracted from Chiaradia (2015); note that high-pressure melts of mafic rocks can easily produce high Sr/Y ratios and might have taken part in the evolution of the granitoids. (d) La/YbN vs. Sr/Y plot, showing the correlation between these ratios as a tool for crustal thickness estimations in magmatic arcs (Profeta et al., 2015). REE were chondrite-normalized (McDonough and Sun, 1995).

evolution with the Southern Brasília Orogen (Henrique-Pinto et al., 2015b) confirmed by the present data. Henrique-Pinto et al. (2012, 2015a,b) denoted a *ca.* 2.2 Ga-old juvenile crust (Mineiro Belt) in the São Francisco Craton as main source area. This juvenile crust overlaps the assumed ~2.45–2.2 Ga period of global magmatic inactivity (Condie et al., 2009; Eriksson and Condie, 2014) leading the authors to propose the southwestward extension of the São Francisco plate. Nevertheless, Partin et al. (2014) disclosed that active-subduction processes during that period left few juvenile signatures due to rapid crust recycling.

Based on the plate reconstruction of Merdith et al. (2017), the Paranapanema and São Francisco blocks were only accreted at 670 Ma (Frugis et al., 2018), making the São Roque Domain part of the Paranapanema active margin. The Cryogenian (and Tonian) zircon record of the São Roque Domain is more likely related to the magmatic arc of Socorro-Guaxupé Nappe, since the Ribeira-Araçuaí belts were recording pre-collisional stages of orogeny after ~650 Ma (Corrales et al., 2020). Moreover, such as in the eastern São Roque Domain, Neoarchean zircon ages with negative $\varepsilon Hf_t$ were found in the north region of the Southern Brasília Orogen and hold evidence of a reworked Neoarchean crust that

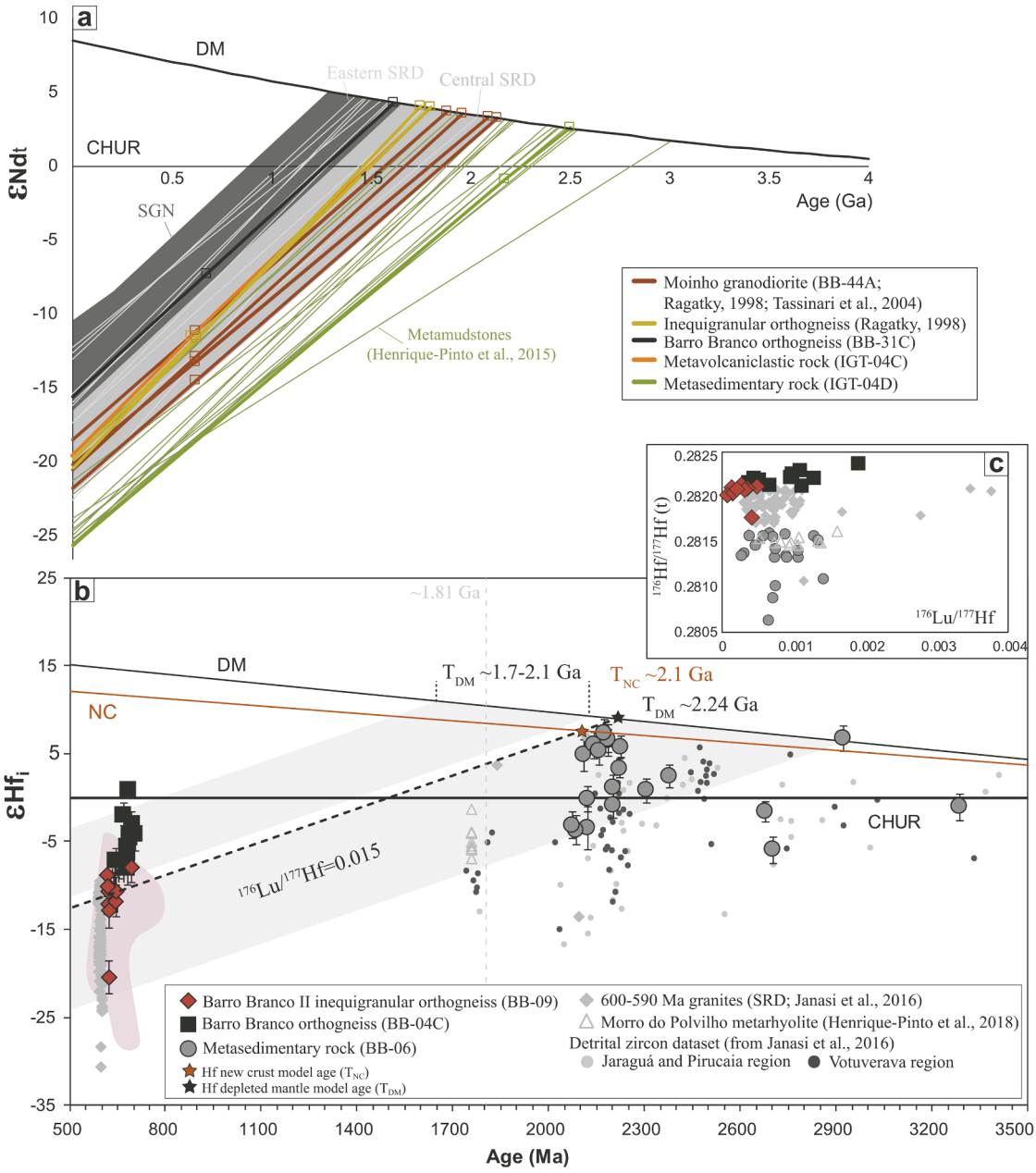


**Fig. 13.** . (a) εNd plot of all sampled rocks with compiled Nd data from metamudstones of the central São Roque Domain (Henrique-Pinto et al., 2015a). (b) $\varepsilon Hf_t$ plot of all sampled rocks. Black dashed line is the $^{176}Lu/^{177}Hf$ = 0.015 crustal evolution (Griffin et al., 2002); orange line is the "new crust" (Dhuime et al., 2011); grey area encompasses the isotopic trend of the Morro do Polvilho metarhyolite (Henrique-Pinto et al., 2018); light grey dashed line marks the youngest detrital zircon from our dataset. The unpublished detrital zircon array was extracted from Fig. 11 in Janasi et al. (2016) for virtual comparison. Pink area includes metatexites (Mora et al., 2014) and granulites (Tedeschi et al., 2018) from the Socorro-Guaxupé Nappe. (c) $^{176}Hf/^{177}Hf(t)$ vs. $^{176}Lu/^{177}Hf$ plot to help identify distinctive isotopic patterns of each sample. (For interpretation of the references to color in this figure legend, the reader is referred to the web version of this article.)

contributed to the magmatism (Tedeschi et al., 2018). We propose the Rhyacian source area potentially lies in the Socorro-Guaxupé basement, thus placing the São Roque Domain in a retro-arc setting.

### 6.4.2. Origin of the high-K magmatism

The origin of the widespread high-K signature of arc-related rocks in the São Roque Domain and surrounding terranes is often associated with an enriched mantle source. We discuss a variety of processes fitting to our scenario that could generate such trend. High-$K_2O$ magmatism can derive from phlogopite-bearing sources at great depths or a K-enriched lower crust exposed by delamination in back-arc domains (e.g., Tatsumi and Eggins, 1995 and references therein; Feldstein and Lange, 1999). Nonetheless, low-degree partial melting of "normal" mantle lithosphere in the Sierra Nevada Batholith was enough to develop high-$K_2O$ through fractional crystallization (Putirka and Busby, 2007). Similarly, the Northern Marianas record shoshonitic low-degree mantle partial melts in the volcanic front (Stern et al., 1988). Continental sediment inputs to the mantle through subduction zones can also generate high-$K_2O$ melts at shallow mantle depths (Wang et al., 2017). The high-K granitoids of the Socorro-Guaxupé-São Roque may be products of low-degree partial melting. However, since such process would rapidly deplete the source, replenishment from sediment-derived melts and/or the contribution from the enriched mantle could play a vital role.

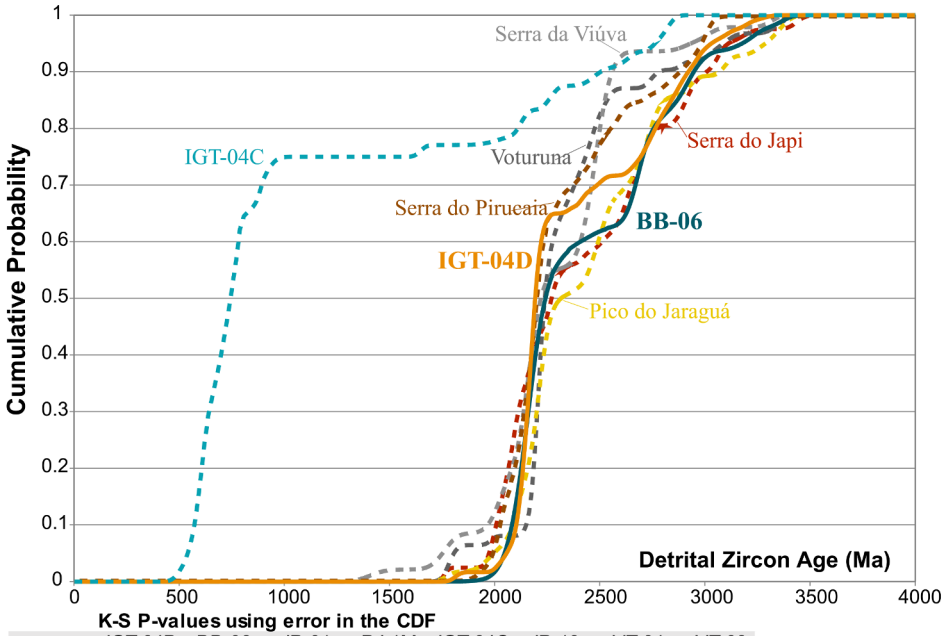


**K-S P-values using error in the CDF**

| | IGT-04D | BB-06 | JP-01 | PJ-1M | IGT-04C | JP-19 | VT-04 | VT-03 |
|---|---|---|---|---|---|---|---|---|
| IGT-04D | | **0.529** | **0.287** | **0.054** | 0.000 | **0.721** | 0.014 | **0.164** |
| BB-06 | **0.529** | | **0.690** | **0.815** | 0.000 | **0.208** | **0.051** | 0.020 |
| JP-01 | **0.287** | **0.690** | | **0.492** | 0.000 | **0.365** | **0.087** | **0.051** |
| PJ-1M | **0.054** | **0.815** | **0.492** | | 0.000 | **0.149** | **0.121** | **0.108** |
| IGT-04C | 0.000 | 0.000 | 0.000 | 0.000 | | 0.000 | 0.000 | 0.000 |
| JP-19 | **0.721** | **0.208** | **0.365** | **0.149** | 0.000 | | 0.049 | **0.737** |
| VT-04 | 0.014 | **0.051** | **0.087** | **0.121** | 0.000 | 0.049 | | **0.064** |
| VT-03 | **0.164** | 0.020 | **0.051** | **0.108** | 0.000 | **0.737** | **0.064** | |

**Fig. 14.** . Cumulative probability curves for sampled metasedimentary rocks (BB-06 and IGT-04D) compared to a metavolcaniclastic rock with important Paleoproterozoic-Archean inherences (IGT-04C), metasandstones (PJ-1M, VT-03, VT-04 and JP-19) from the São Roque Domain, and one sample from the Socorro-Guaxupé Nappe (JP-01) (Henrique-Pinto et al., 2015b). The K-S test run for the samples results in P-values that measure the degree in which zircon populations are *not* different (Guynn and Gehrels, 2010). Bold values assign all P > 0.05 (95% confidence level) and orange boxes indicate the higher P-values for each sample pair. (For interpretation of the references to color in this figure legend, the reader is referred to the web version of this article.)

### 6.5. Tectonic evolution

The subduction configuration is the prime reason for the magmatic distribution in space and time (Cross and Pilger, 1982; Nakajima and Hasegawa, 2007). Considering the southwestern-driven subduction underneath the Paranapanema plate, the São Roque Domain presents a consistent structural framework and chrono-correlations with the Socorro-Guaxupé Nappe that favor a retro-arc setting (Fig. 15a). Following the 685–675 Ma Barro Branco event (and possible Tonian activity from a metavolcaniclastic rock), the São Roque Domain documented a magmatic gap of ~40–80 m.y. (considering age uncertainties). During this period, the Socorro-Guaxupé domain recorded extensive, north-northwestward arc-related magmatism and a syn-collisional UHT metamorphism from 670 to 590 Ma (Haddad, 1995; Gengo, 2014; Mora et al., 2014; Vinagre et al., 2014). We hypothesize that during this period the subduction geometry beneath the Paranapanema plate shifted. Steepening of the subduction angle (slab rollback; e.g., Hawkins, 1995; Kincaid and Griffiths, 2003; Ramos, 2010; Munch et al., 2020) supports the interruption of magmatism in the retro-arc and the northward migration to the arc domain (Fig. 15b). Relaxation of the subduction angle leading to the emplacement of the Ediacaran granitoids in the retro-arc is concomitant with the collisional stage in the neighbor domain (Rocha et al., 2017; Tedeschi et al., 2018) (Fig. 15c). The period is marked by more evolved geochemical and isotopic compositions. Growth of metamorphic monazite at *ca.* 600 Ma (and two monazite cores of *ca.* 630 Ma) coincides with zircon and monazite ages of syn-collisional partial melting and last stages of melt crystallization in the Socorro-Guaxupé Nappe (Martins et al., 2009; Rocha et al., 2017; Tedeschi et al., 2018).

Considering the last-longing subduction beneath the Paranapanema (Frugis et al., 2018; Tedeschi et al., 2018), subduction erosion could have fed trench sediments and/or fore-arc crust (e.g., Andrelândia schists) into the mantle. Aside from enriching the mantle, the eroded material may rise as melts and relaminate to the base of the crust (e.g., Castro, 2014; Kelemen and Behn, 2016; Ewing et al., 2018) adding a crustal component to the source of magmatism.

## 7. Conclusions

This research provides unprecedented data concerning the eastern São Roque Domain and proposes a tectonic model based on geochemical and chronological constraints. The widespread subduction-related high-K calc-alkaline magmatism and age correlations throughout the São Roque Domain and neighbor Socorro-Guaxupé Nappe support a joint tectonic evolution. The Barro Branco orthogneiss is a major folded I-type granitoid dated at *ca.* 680 Ma with a juvenile component. Associated granitoids formed at *ca.* 625 Ma and 620 Ma with crustal Hf-Nd signatures indicating progressively mixed mantle and crustal sources for the granite magmatism. Bulk-rock geochemistry suggests a main parental source derived from the lower crust, yielding high Sr/Y and La/Yb due to residual deep-seated assemblages (e.g., garnet ± clinopyroxene ± amphibole).

Inherited zircon grains span from Paleoproterozoic to Archean. A metavolcaniclastic rock presented a remarkable age spectrum from 700 Ma to 800–900 Ma, the latter reported for the first time in this domain. Provenance of detrital zircon yielded a Rhyacian peak at *ca.* 2.17 Ga that is consistent with observed patterns in the central São Roque Domain and southern region of the Socorro-Guaxupé, thus, linking their evolution. Monazite U-Pb reported a metamorphic episode at ca. 600 Ma (possibly initiated around 630 Ma), concomitant with the 630–590 Ma metamorphism in the Socorro-Guaxupé Nappe.

We propose the Barro Branco orthogneiss records an early magmatism in the retro-arc domain during the initiation of subduction beneath the Paranapanema active margin. Magmatism in the São Roque Domain potentially derived from a *ca.* 2.1 Ga juvenile crust that lies within the Paranapanema block. Slab rollback caused the magmatism to migrate northwards resulting in a ~40–80 m.y. magmatic gap in the retro-arc domain. Relaxation of the subducting slab (Barro Branco II

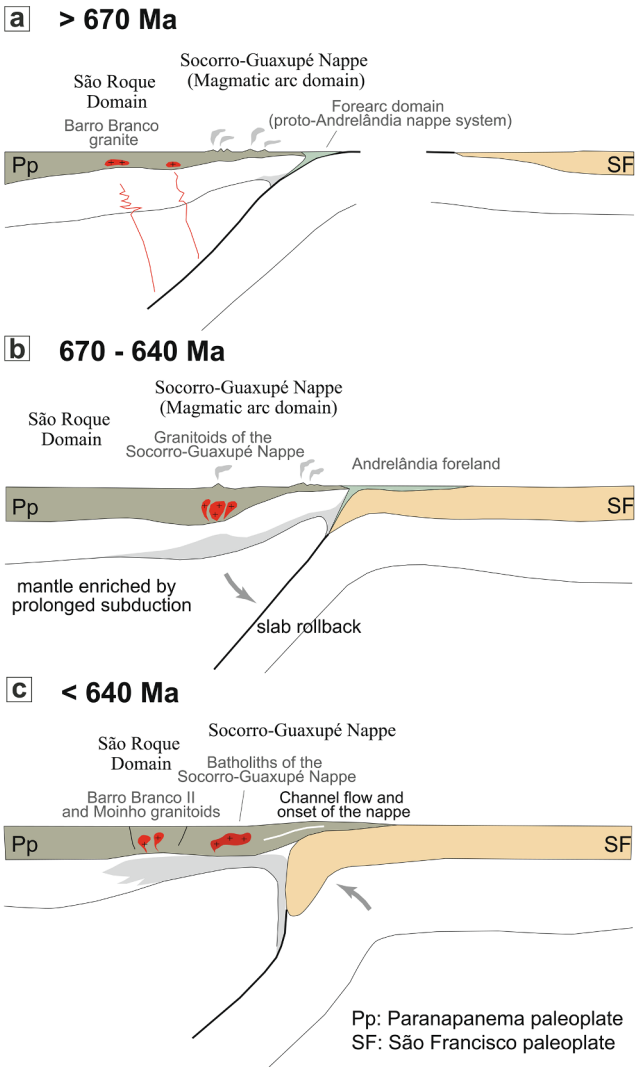


**Fig. 15.** . Schematic tectonic model based on the proposed evolution for the São Roque Domain in a retro-arc setting regarding the convergence between the Paranapanema and São Francisco paleoplates. The model is divided into three main stages (a–c) anchored on the geochronological constraints here presented and studies from the surrounding tectonic domains.

and Moinho granodiorite) relates to the continental collision between the Paranapanema and São Francisco paleoplates. Contamination from the metasedimentary sequence and crustal additions to the source (re-lamination?) during the last-longing subduction left evolved isotopic imprints. The retro-arc São Roque Domain as part of the Southern Brasília Orogen history contributes to the record of the West-Gondwana assembly in southeastern Brazil.

## CRediT authorship contribution statement

**Mikaella Balis:** Conceptualization, Methodology, Validation, Formal analysis, Investigation, Writing - original draft, Visualization. **Mario da Costa Campos Neto:** Conceptualization, Methodology, Validation, Investigation, Resources, Writing - review & editing, Visualization, Supervision, Project administration, Funding acquisition. **Adriana Alves:** Conceptualization, Validation, Writing - review & editing, Supervision.

## Declaration of Competing Interest

The authors declare that they have no known competing financial interests or personal relationships that could have appeared to influence the work reported in this paper.

## Acknowledgements

The authors would like to thank the two anonymous reviewers for their insightful comments and suggestions that greatly contributed to the improvement of the manuscript, and W. Teixeira and E.P. Oliveira for the editorial handling. The authors are also grateful to the CPGeo and NAP-Geoanalítica staff (Institute of Geosciences, University of São Paulo) for assisting with analytical procedures. This research was supported by the São Paulo Research Foundation (FAPESP Grant 2015/03737-0). M.C. Campos Neto is a CNPq researcher (National Council for Scientific and Technological Development) and M. Balis received an MSc scholarship from CAPES.

## Appendix A. Supplementary data

Supplementary data to this article can be found online at https://doi.org/10.1016/j.precamres.2020.105913.

## References

Aleinikoff, J.N., Schenck, W.S., Plank, M.O., Srogi, L.A., Fanning, C.M., Kamo, S.L., Bosbyshell, H., 2006. Deciphering igneous and metamorphic events in high-grade rocks of the Wilmington complex, Delaware: morphology, cathodoluminescence and backscattered electron zoning, and SHRIMP U-Pb geochronology of zircon and monazite. Bull. Geol. Soc. Am. 118, 39–64. https://doi.org/10.1130/B25659.1.

Alkmim, F.F., Kuchenbecker, M., Reis, H.L.S., Pedrosa-Soares, A.C., 2017. The Araçuaí Belt. In: Heilbron, M., Cordani, U.G., Alkmim, F.F. (Eds.), São Francisco Craton. Springer International Publishing, Eastern Brazil, pp. 255–276. https://doi.org/10.1007/978-3-319-01715-0_14.

Alves, A., Janasi, V.A., Campos Neto, M.C., Heaman, L., Simonetti, A., 2013. U-Pb geochronology of the granite magmatism in the Embu Terrane: implications for the evolution of the Central Ribeira Belt, SE Brazil. Precambr. Res. 230, 1–12. https://doi.org/10.1016/j.precamres.2013.01.018.

Alves, A., Janasi, V.A., Campos Neto, M.C., 2016. Sources of granite magmatism in the Embu Terrane (Ribeira Belt, Brazil): neoproterozoic crust recycling constrained by elemental and isotope (Sr-Nd-Pb) geochemistry. J. S. Am. Earth Sci. 68, 205–223. https://doi.org/10.1016/j.jsames.2015.10.014.

Amaral, L., Caxito, F.A., Pedrosa-Soares, A.C., Queiroga, G., Babinski, M., Trindade, R., Lana, C., Chemale, F., 2020. The Ribeirão da Folha ophiolite-bearing accretionary wedge (Araçuaí orogen, SE Brazil): new data for Cryogenian plagiogranite and metasedimentary rocks. Precambr. Res. 336, 105522. https://doi.org/10.1016/j.precamres.2019.105522.

Bergmann, M., 1988. Caracterização estratigráfica e estrutural da sequência Vulcano-sedimentar do Grupo São Roque – na região de Pirapora do Bom Jesus -. Estado de São Paulo. University of São Paulo.

Blatter, D.L., Carmichael, I.S.E., Deino, A.L., Renne, P.R., 2001. Neogene volcanism at the front of the Central Mexican volcanic belt: basaltic andesites to dacites, with contemporaneous shoshonites and high-TiO2 lava. Bull. Geol. Soc. Am. 113, 1324–1342. https://doi.org/10.1130/0016-7606(2001)113<1324:NVATFO>2.0.CO;2.

Blichert-Toft, J., Chauvel, C., Albarède, F., 1997. Separation of Hf and Lu for high-precision isotope analysis of rock samples by magnetic sector-multiple collector ICP-MS. Contrib. Miner. Petrol. 127, 248–260. https://doi.org/10.1007/s004100050278.

Bouvier, A., Vervoort, J.D., Patchett, P.J., 2008. The Lu-Hf and Sm-Nd isotopic composition of CHUR: constraints from unequilibrated chondrites and implications for the bulk composition of terrestrial planets. Earth Planet. Sci. Lett. 273, 48–57. https://doi.org/10.1016/j.epsl.2008.06.010.

Brito Neves, B.B., Campos Neto, M.C., Fuck, R.A., 1999. From Rodinia to western Gondwana; an approach to the Brasiliano-Pan African cycle and orogenic collage. Episodes 22, 155–166. https://doi.org/10.1016/j.precamres.2007.04.018.

Broska, I., Siman, P., 1998. The breakdown of monazite in the west-carpathian veporic orthogneisses and tatric granites. Geol. Carpath. 49, 161–167.

Campanha, G.A.C., Faleiros, F.M., Cawood, P.A., Cabrita, D.I.G., Ribeiro, B.V., Basei, M.A.S., 2019. The Tonian Embu Complex in the Ribeira Belt (Brazil): revision, depositional age and setting in Rodinia and West Gondwana. Precambr. Res. 320, 31–45. https://doi.org/10.1016/j.precamres.2018.10.010.

Campos Neto, M.C., 2000. Orogenic systems from Southwestern Gondwana: an approach to Brasiliano-Pan African cycle and orogenic collage in southeastern Brazil. Tectonic Evol. S. Am. 335–365.

Campos Neto, M.C., Basei, M.A.S., Artur, A.C., Silva, M.E., Machado, R., Dias Neto, C.M., Fragoso César, A.R., 1983. Geologia das folhas Piracaia e Igaratá. São Paulo.

Campos Neto, M.C., Basei, M.A.S., Bergmann, M., 1988. Geologia da Folha Ribeirão do Engenho 1:25000. São Paulo.

Campos Neto, M.C., Caby, R., 1999. Neoproterozoic high-pressure metamorphism and tectonic constraint from the nappe system south of the São Francisco. Precambr. Res. 97, 3–26.

Campos Neto, M.C., Caby, R., 2000. Terrane accretion and upward extrusion of high-

pressure granulites in the Neoproterozoic nappes of southeast Brazil : petrologic and structural constraints. Tectonics 19, 669–687.
Campos Neto, M.C., Cioffi, C.R., Moraes, R., Motta, R.G., Siga Jr., O., Basei, M.A.S., 2010. Structural and metamorphic control on the exhumation of high- P granulites : the Carvalhos Klippe example, from the oriental Andrelândia Nappe System, southern portion of the Brasília Orogen, Brazil. Precambr. Res. 180, 125–142. https://doi.org/10.1016/j.precamres.2010.05.010.
Campos Neto, M.C., Basei, M.A.S., Janasi, V.A., Moraes, R., 2011. Orogen migration and tectonic setting of the Andrelândia Nappe system: an Ediacaran western Gondwana collage, south of São Francisco craton. J. S. Am. Earth Sci. 32, 393–406. https://doi.org/10.1016/j.jsames.2011.02.006.
Castro, A., 2014. The off-crust origin of granite batholiths. Geosci. Front. 5, 63–75. https://doi.org/10.1016/j.gsf.2013.06.006.
Catlos, E.J., 2013. Generalizations about monazite: implications for geochronologic studies. Am. Mineral. 98, 819–832. https://doi.org/10.2138/am.2013.4336.
Chiaradia, M., 2015. Crustal thickness control on Sr/Y signatures of recent arc magmas: an Earth scale perspective. Sci. Rep. 5, 8115. https://doi.org/10.1038/srep08115.
Chu, N.C., Taylor, R.N., Chavagnac, V., Nesbitt, R.W., Boella, R.M., Milton, J.A., German, C.R., Bayon, G., Burton, K., 2002. Hf isotope ratio analysis using multi-collector inductively coupled plasma mass spectrometry: an evaluation of isobaric interference corrections. J. Anal. At. Spectrom. 17, 1567–1574. https://doi.org/10.1039/b206707b.
Cioffi, C.R., Campos Neto, M.C., Möller, A., Rocha, B.C., 2016a. Tectonic significance of the Meso- to Neoarchean complexes in the basement of the southern Brasília Orogen. Precambr. Res. 287, 91–107. https://doi.org/10.1016/j.precamres.2016.10.009.
Cioffi, C.R., Campos Neto, M.C., Möller, A., Rocha, B.C., 2016b. Paleoproterozoic continental crust generation events at 2.15 and 2.08Ga in the basement of the southern Brasília Orogen, SE Brazil. Precambr. Res. 275, 176–196. https://doi.org/10.1016/j.precamres.2016.01.007.
Cioffi, C.R., Campos Neto, M.C., Möller, A., Rocha, B.C., 2019. Titanite petrochronology of the southern Brasília Orogen basement: effects of retrograde net-transfer reactions on titanite trace element compositions. Lithos 344–345, 393–408. https://doi.org/10.1016/j.lithos.2019.06.035.
Coelho, M.B., Trouw, R.A.J., Ganade, C.E., Vinagre, R., Mendes, J.C., Sato, K., 2017. Constraining timing and P-T conditions of continental collision and late overprinting in the Southern Brasília Orogen (SE-Brazil): U-Pb zircon ages and geothermobarometry of the Andrelândia Nappe System. Precambr. Res. 292, 194–215. https://doi.org/10.1016/j.precamres.2017.02.001.
Condie, K.C., O'Neill, C., Aster, R.C., 2009. Evidence and implications for a widespread magmatic shutdown for 250 My on Earth. Earth Planet. Sci. Lett. 282, 294–298. https://doi.org/10.1016/j.epsl.2009.03.033.
Cordani, U.G., Coutinho, J.M.V., Nutman, A.P., 2002. Geochronological constraints on the evolution of the Embu Complex, São Paulo, Brazil. J. S. Am. Earth Sci. 14, 903–910. https://doi.org/10.1016/S0895-9811(01)00083-9.
Corrales, F.F.P., Dussin, I.A., Heilbron, M., Bruno, H., Bersan, S., Valeriano, C.M., Pedrosa-Soares, A.C., Tedeschi, M., 2020. Coeval high Ba-Sr arc-related and OIB Neoproterozoic rocks linking pre-collisional magmatism of the Ribeira and Araçuaí orogenic belts, SE-Brazil. Precambr. Res. 337, 105476. https://doi.org/10.1016/j.precamres.2019.105476.
Corrie, S.L., Kohn, M.J., 2008. Trace-element distributions in silicates during prograde metamorphic reactions: implications for monazite formation. J. Metamorph. Geol. 26, 451–464. https://doi.org/10.1111/j.1525-1314.2008.00769.x.
Cross, T.A., Pilger, R.E.X.H., 1982. Controls of subduction geometry, location of magmatic arcs, and tectonics of arc and back-arc regions. Geol. Soc. Am. Bull. 7606. https://doi.org/10.1130/0016-7606(1982)93<545.
Davidson, J., Turner, S., Handley, H., Macpherson, C., Dosseto, A., 2007. Amphibole "sponge" in arc crust? Geology 35, 787. https://doi.org/10.1130/G23637A.1.
Defant, M.J., Drummond, M.S., 1990. Derivation of some modern arc magmas by melting of young subducted lithosphere. Nature 347, 662–665. https://doi.org/10.1038/347662a0.
Degler, R., Pedrosa-Soares, A.C., Dussin, I.A., Queiroga, G., Schulz, B., 2017. Contrasting provenance and timing of metamorphism from paragneisses of the Araçuaí-Ribeira orogenic system, Brazil: hints for Western Gondwana assembly. Gondwana Res. 51. https://doi.org/10.1016/j.gr.2017.07.004.
DePaolo, D.J., 1981. Neodymium isotopes in the Colorado Front Range and crust–mantle evolution in the Proterozoic. Nature 291, 193–196. https://doi.org/10.1038/291193a0.
Dhuime, B., Hawkesworth, C., Cawood, P., 2011. When continents formed. Science 331, 154–155. https://doi.org/10.1126/science.1201245.
Ducea, M.N., Saleeby, J.B., Bergantz, G., 2015. The architecture, chemistry, and evolution of continental magmatic arcs. Annu. Rev. Earth Planet. Sci. 43, 299–331. https://doi.org/10.1146/annurev-earth-060614-105049.
Ebert, H.D., Chemale, F., Babinski, M., Schmus, W.R.V., 1996. Tectonic setting and U / Pb zircon dating of the plutonic Socorro Complex in the Transpressive. Tectonics 15, 688–699.
Elhlou, S., Belousova, E., Griffin, W.L., Pearson, N.J., O'Reilly, S.Y., 2006. Trace element and isotopic composition of GJ-red zircon standard by laser ablation. Geochim. Cosmochim. Acta 70, A158. https://doi.org/10.1016/j.gca.2006.06.1383.
Eriksson, P.G., Condie, K.C., 2014. Cratonic sedimentation regimes in the ca. 2450–2000Ma period: relationship to a possible widespread magmatic slowdown on Earth? Gondwana Res. 25, 30–47. https://doi.org/10.1016/j.gr.2012.08.005.
Ewing, T.A., Müntener, O., Leuthold, J., Arellano, C.R., Baumgartner, L.P., Schaltegger, U., 2018. The zircon Hf isotope archive of rapidly changing mantle sources in the south Patagonian retro-arc. Bull. Geol. Soc. Am. 131, 587–608. https://doi.org/10.1130/B31983.1.
Feldstein, S.N., Lange, R.A., 1999. Pliocene potassic magmas from the Kings River region, Sierra Nevada, California: evidence for melting of a subduction-modified mantle. J. Petrol. 40, 1301–1320. https://doi.org/10.1093/petroj/40.8.1301.
Fernandes, G.L.F., Schmitt, R.S., Bongiolo, E.M., Basei, M.A.S., Mendes, J.C., 2015. Unraveling the tectonic evolution of a Neoproterozoic-Cambrian active margin in the Ribeira Orogen (Se Brazil): U-Pb and Lu–Hf provenance data. Precambr. Res. https://doi.org/10.1016/j.precamres.2015.05.017.
Finger, F., Broska, I., Roberts, M.P., Schermaier, A., 1998. Replacement of primary monazite by apatite-allanite-epidote coronas in an amphibolite facies granite gneiss from the eastern Alps. Am. Mineral. 83, 248–258. https://doi.org/10.2138/am-1998-3-408.
Fossen, H., Cavalcante, C., Konopásek, J., Meira, V.T., de Almeida, R.P., Hollanda, M.H.B.M., Trompette, R., 2020. A critical discussion of the subduction-collision model for the Neoproterozoic Araçuaí-West Congo orogen. Precambr. Res. 343. https://doi.org/10.1016/j.precamres.2020.105715.
Frisch, W., Meschede, M., Blakey, R.C., 2011. In: Plate Tectonics, Plate Tectonics: Continental Drift and Mountain Building. Springer Berlin Heidelberg, Berlin, Heidelberg. https://doi.org/10.1007/978-3-540-76504-2.
Frost, B.R., Barnes, C.G., Collins, W.J., Arculus, R.J., Ellis, D.J., Frost, C.D., 2001. A geochemical classification for granitic rocks. J. Petrol. 42, 2033–2048. https://doi.org/10.1093/petrology/42.11.2033.
Frugis, G.L., Campos Neto, M.C., Bittencourt, R., 2018. Eastern Paranapanema and Southern São Francisco orogenic margins-Records of enduring Neoproterozoic oceanic convergence and collision in the Southern Brasília Orogen. Precambr. Res. 35–57.
Fuck, R.A., Pimentel, M.M., Alvarenga, C.J.S., Dantas, E.L., 2017. The Northern Brasília Belt. In: São Francisco Craton, Eastern Brazil. pp. 205–220. https://doi.org/10.1007/978-3-319-01715-0_11.
Fumes, R.A., Luvizotto, G.L., Moraes, R., Heilbron, M., Vlach, S.R.F., 2019. Metamorphic modeling and petrochronology of metapelitic rocks from the Luminárias Nappe, southern Brasília belt (SE Brazil). Braz. J. Geol. 49. https://doi.org/10.1590/2317-4889201920180114.
Garcia, M.G.M., Campos Neto, M.C., 1997. Superposição Destral Em Ampla Zona De Cisalhamento Sinistral: Cinturão De Cisalhamento São Paulo, Imediações De Piracaia - SP. Rev. Bras. Geociências 27, 339–348. https://doi.org/10.25249/0375-7536.1997339348.
Gengo, R.M., 2014. Petrologia de ortognaisses e granitoides do Domínio Socorro, Nappe Socorro-Guaxupé, seção Extrema-Camanducaia. University of São Paulo.
Griffin, W.L., Wang, X., Jackson, S.E., Pearson, N.J., O'Reilly, S.Y., Xu, X., Zhou, X., 2002. Zircon chemistry and magma mixing, SE China: in-situ analysis of Hf isotopes, Tonglu and Pingtan igneous complexes. Lithos 61, 237–269. https://doi.org/10.1016/S0024-4937(02)00082-8.
Guynn, J., Gehrels, G., 2010. Comparison of Detrital Zircon Age Distributions Using the K-S Test. Manual 1–16.
Hackspacher, P.C., Dantas, E.L., Spoladore, A., Fetter, A.H., Aurélio, M., Oliveira, F.D.E., 2000. Evidence of Neoproterozoic back-arc basin development in the Central Ribeira Belt, southeastern Brazil: new geochronological and geochemical constraints from the São Roque - Açungui Groups. Rev. Bras. Geociências 30, 110–114.
Hackspacher, P.C., Fetter, A.H., Ebert, H.D., Janasi, V.A., Dantas, E.L., Oliveira, M.A.F., Braga, I.F., Negri, F.A., 2003. Magmatismo há ca. 660–640 Ma no Domínio Socorro: Registros de convergência-colisional na Aglutinação do Gondwana Ocidental. Geologia USP - Serie Cientifica 3, 85–96.
Haddad, R.C., 1995. O Batólito Granitoide Pinhal-Ipuiúna (SP-MG): Um exemplo do magmatismo cálcio-alcalino potássico neoproterozoico no sudeste brasileiro. Universidade de São Paulo.
Hamilton, P.J., O'Nions, R.K., Bridgwater, D., Nutman, A., 1983. Sm-Nd studies of Archaean metasediments and metavolcanics from West Greenland and their implications for the Earth's early history. Earth Planet. Sci. Lett. 62, 263–272. https://doi.org/10.1016/0012-821X(83)90089-4.
Harrison, T.M., Watson, E.B., 1984. The behavior of apatite during crustal anatexis: equilibrium and kinetic considerations. Geochim. Cosmochim. Acta 48, 1467–1477. https://doi.org/10.1016/0016-7037(84)90403-4.
Hawkins, J.W., 1995. The Geology of the Lau Basin,. In: Taylor, B. (Ed.), Backarc Basins. Springer US, Boston, MA, pp. 63–138. https://doi.org/10.1007/978-1-4615-1843-3_3.
Heilbron, M., Cordani, U.G., Alkmim, F.F., 2017a. In: São Francisco Craton, Eastern Brazil. Springer, Regional Geology Reviews. Springer International Publishing, Cham. https://doi.org/10.1007/978-3-319-01715-0.
Heilbron, M., Ribeiro, A., Valeriano, C.M., Paciullo, F.V., Almeida, J.C.H., Trouw, R.A.J., Tupinambá, M., Eirado Silva, L.G., 2017b. The Ribeira Belt, in: São Francisco Craton, Eastern Brazil. pp. 277–302. https://doi.org/10.1007/978-3-319-01715-0_15.
Heilbron, M., Machado, N., 2003. Timing of terrane accretion in the Neoproterozoic-Eopaleozoic Ribeira Orogen (se Brazil). Precambr. Res. 125, 87–112. https://doi.org/10.1016/S0301-9268(03)00082-2.
Heilbron, M., Tupinambá, M., Valeriano, C.M., Armstrong, R., Siva, L.G.E., Melo, R.S., Simonetti, A., Pedrosa-Soares, A.C., Machado, N., 2013. The Serra da Bolívia complex: the record of a new Neoproterozoic arc-related unit at Ribeira belt. Precambr. Res. 238, 158–175. https://doi.org/10.1016/j.precamres.2013.09.014.
Heilbron, M., Valeriano, C.M., Peixoto, C., Tupinambá, M., Neubauer, F., Dussin, I., Corrales, F., Bruno, H., Lobato, M., Horta de Almeida, J.C., Guilherme do Eirado Silva, L., 2020. Neoproterozoic magmatic arc systems of the central Ribeira belt, SE-Brazil, in the context of the West-Gondwana pre-collisional history: a review. J. S. Am. Earth Sci. 103. https://doi.org/10.1016/j.jsames.2020.102710.
Henrique-Pinto, R., Janasi, V.A., Simonetti, A., Tassinari, C.C.G., Heaman, L.M., 2012. Paleoproterozoic source contributions to the São Roque Group sedimentation: LA-MC-ICPMS U-Pb dating and Sm-Nd systematics of clasts from metaconglomerates of the Boturuna Formation. Geologia USP - Serie Cientifica 12, 21–32. https://doi.org/

10.5327/Z1519-874X2012000300002.
Henrique-Pinto, R., Janasi, V.A., Tassinari, C.C.G., Carvalho, B.B., Cioffi, C.R., Stríkis, N.M., 2015a. Provenance and sedimentary environments of the Proterozoic São Roque Group, SE-Brazil: contributions from petrography, geochemistry and Sm–Nd isotopic systematics of metasedimentary rocks. J. S. Am. Earth Sci. 63, 191–207. https://doi.org/10.1016/j.jsames.2015.07.015.
Henrique-Pinto, R., Janasi, V.A., Vasconcellos, A.C.B.C., Sawyer, E.W., Barnes, S.-J., Basei, M.A.S., Tassinari, C.C.G., 2015b. Zircon provenance in meta-sandstones of the São Roque Domain: implications for the Proterozoic evolution of the Ribeira Belt, SE Brazil. Precambr. Res. 256, 271–288. https://doi.org/10.1016/j.precamres.2014.11.014.
Henrique-Pinto, R., Janasi, V.A., Campanha, G.A.C., 2018. U-Pb dating, Lu-Hf isotope systematics and chemistry of zircon from the Morro do Polvilho meta-trachydacite: constraints on sources of magmatism and on the depositional age of the São Roque Group. Geologia USP. Série Científica 18, 45–56. https://doi.org/10.11606/issn.2316-9095.v18-125793.
Janasi, V.A., 1999. Petrogênese de Granitos Crustais da Nappe de Empurrão Socorro-Guaxupé (SP-MG): uma contribuição da Geoquímica Elemental e Isotópica. University of São Paulo.
Janasi, V.A., Ulbrich, H.H.G.J., 1991. Late Proterozoic granitoid magmatism in the state of São Paulo, southeastern Brazil. Precambr. Res. 51, 351–374.
Janasi, V.A., Andrade, S., Vasconcellos, A.C.B.C., Henrique-Pinto, R., Ulbrich, H.H.G.J., 2016. Timing and sources of granite magmatism in the Ribeira Belt, SE Brazil : in-sights from zircon in situ U e Pb dating and Hf isotope geochemistry in granites from the São Roque Domain. J. S. Am. Earth Sci. 68, 224–247. https://doi.org/10.1016/j.jsames.2015.11.009.
Janoušek, V., Farrow, C.M., Erban, V., 2006. Interpretation of whole-rock geochemical data in igneous geochemistry: introducing Geochemical Data Toolkit (GCDkit). J. Petrol. 47, 1255–1259. https://doi.org/10.1093/petrology/egl013.
Juliani, C., Beljavskis, P., 1995. Revisão da litoestratigrafia da Faixa São Roque/Serra do Itaberaba (SP). Rev. Inst. Geol. 16, 33–58.
Juliani, C., Beljavskis, P., Schorscher, J.H.D., 1986. Petrogênese do vulcanismo e aspectos metalogenéticos associados: Grupo Serra do Itaberaba na região do São Roque – SP, Congresso Brasileiro de Geologia. Goiânia 730–747.
Juliani, C., Hackspacher, P., Dantas, E.L., Fetter, A.H., 2000. The Mesoproterozoic Volcano-Sedimentary Serra Do Itaberaba Group Of The Central Ribeira Belt, São Paulo State, Brazil: implications For The Age Of The Overlying São Roque Group. Rev. Bras. Geociências 30, 82–86.
Juliani, C., 1993. Geologia, petrogênese e aspectos metalogenéticos dos Grupos Serra do Itaberaba e São Roque na região das serras do Itaberaba e da Pedra Branca, NE da cidade de São Paulo, SP. 703.
Kelemen, P.B., Behn, M.D., 2016. Formation of lower continental crust by relamination of buoyant arc lavas and plutons. Nat. Geosci. 9, 197–205. https://doi.org/10.1038/ngeo2662.
Kincaid, C., Griffiths, R.W., 2003. Laboratory models of the thermal evolution of the mantle during rollback subduction. Nature 425, 58–62. https://doi.org/10.1038/nature01923.
Lamoso, I.S.M., Janasi, V.A., 2019. SHRIMP U-Pb zircon dating of Neoproterozoic granites from the easternmost São Roque Domain, Ribeira Belt. Geologia USP. Série Científica 19, 55–75. https://doi.org/10.11606/issn.2316-9095.v19-148374.
Linthout, K., 2007. Tripartite division of the system 2REEPO4-CaTh (PO4)2–2ThSiO4, discreditation of brabantite, and recognition of cheralite as the name for members dominated by CaTh(PO4)2. Can. Mineral. 45, 503–508. https://doi.org/10.2113/gscanmin.45.3.503.
Ludwig, K.R., 2003. Isoplot 3.00: A geochronological toolkit for Microsoft Excel.
Marimon, R.S., Trouw, R.A.J., Dantas, E.L., Ribeiro, A., 2020. U-Pb and Lu-Hf isotope systematics on detrital zircon from the southern São Francisco Craton's Neoproterozoic passive margin: Tectonic implications. J. S. Am. Earth Sci. 100, 102539. https://doi.org/10.1016/j.jsames.2020.102539.
Martins, L., Vlach, S.R.F., Janasi, V.A., 2009. Reaction microtextures of monazite: correlation between chemical and age domains in the Nazaré Paulista migmatite, SE Brazil. Chem. Geol. 261, 271–285. https://doi.org/10.1016/j.chemgeo.2008.09.020.
Maurer, V.C., 2016. Caracterização geocronológica (U-Pb), geoquímica e isotópica (Sr, Nd, Hf) do Complexo Rio Capivari no Terreno Embu. Universidade de São Paulo.
McDonough, W.F., Sun, S., 1995. The composition of the Earth. Chem. Geol. 120, 223–253. https://doi.org/10.1016/0009-2541(94)00140-4.
Meira, V.T., García-Casco, A., Juliani, C., Almeida, R.P., Schorscher, J.H.D., 2015. The role of intracontinental deformation in supercontinent assembly: insights from the Ribeira Belt, Southeastern Brazil (Neoproterozoic West Gondwana). Terra Nova 27, 206–217. https://doi.org/10.1111/ter.12149.
Merdith, A.S., Collins, A.S., Williams, S.E., Pisarevsky, S., Foden, J.D., Archibald, D.B., Blades, M.L., Alessio, B.L., Armistead, S., Plavsa, D., Clark, C., Müller, R.D., 2017. A full-plate global reconstruction of the Neoproterozoic. Gondwana Res. https://doi.org/10.1016/j.gr.2017.04.001.
Middlemost, E.A.K., 1994. Naming materials in the magma/igneous rock system. Earth-Sci. Rev. 37, 215–224. https://doi.org/10.1016/0012-8252(94)90029-9.
Miller, J.S., Matzel, J.E.P., Miller, C.F., Burgess, S.D., Miller, R.B., 2007. Zircon growth and recycling during the assembly of large, composite arc plutons. J. Volcanol. Geoth. Res. 167, 282–299. https://doi.org/10.1016/j.jvolgeores.2007.04.019.
Mora, C.A.S., Campos Neto, M.C., Basei, M.A.S., 2014. Syn-collisional lower continental crust anatexis in the Neoproterozoic Socorro-Guaxupé Nappe System, southern Brasília Orogen, Brazil: constraints from zircon U-Pb dating, Sr–Nd–Hf signatures and whole-rock geochemistry. Precambr. Res. 255, 847–864. https://doi.org/10.1016/j.precamres.2014.10.017.
Mori, P.E., Reeves, S., Correia, C.T., Haukka, M., 1999. Development of a fused glass disc XRF facility and comparison with the pressed powder pellet technique at Instituto de Geociencias, Sao Paulo University. Rev. Brasil. Geocienc. 29, 441–446. https://doi.org/10.5327/rbg.v29i3.715.
Moyen, J.F., 2009. High Sr/Y and La/Yb ratios: the meaning of the "adakitic signature". Lithos 112, 556–574. https://doi.org/10.1016/j.lithos.2009.04.001.
Munch, J., Gerya, T., Ueda, K., 2020. Oceanic crust recycling controlled by weakening at slab edges. Nat. Commun. 11. https://doi.org/10.1038/s41467-020-15750-7.
Nakajima, J., Hasegawa, A., 2007. Subduction of the Philippine Sea plate beneath southwestern Japan: slab geometry and its relationship to arc magmatism. J. Geophys. Res. Solid Earth 112, 1–18. https://doi.org/10.1029/2006JB004770.
Navarro, M.S., Andrade, S., Ulbrich, H., Gomes, C.B., Girardi, V.A.V., 2008. The direct determination of rare earth elements in basaltic and related rocks using ICP-MS: testing the efficiency of microwave oven sample decomposition procedures. Geostand. Geoanal. Res. 32, 167–180. https://doi.org/10.1111/j.1751-908X.2008.00840.x.
Novo, T.A., Pedrosa-Soares, A.C., Vieira, V.S., Dussin, I., Silva, L.C., 2018. The Rio Doce Group revisited: an Ediacaran arc-related volcano-sedimentary basin, Araçuaí orogen (SE Brazil). J. S. Am. Earth Sci. 85, 345–361. https://doi.org/10.1016/j.jsames.2018.05.013.
Ondrejka, M., Uher, P., Putiš, M., Broska, I., Bačík, P., Konečný, P., Schmiedt, I., 2012. Two-stage breakdown of monazite by post-magmatic and metamorphic fluids: an example from the Veporic orthogneiss, Western Carpathians, Slovakia. Lithos 142–143, 245–255. https://doi.org/10.1016/j.lithos.2012.03.012.
Partin, C.A., Bekker, A., Sylvester, P.J., Wodicka, N., Stern, R.A., Chacko, T., Heaman, L.M., 2014. Filling in the juvenile magmatic gap: evidence for uninterrupted Paleoproterozoic plate tectonics. Earth Planet. Sci. Lett. 388, 123–133. https://doi.org/10.1016/j.epsl.2013.11.041.
Passarelli, C.R., Verma, S.K., McReath, I., Basei, M.A.S., Siga Jr., O., 2019. Tracing the history from Rodinia break-up to the Gondwana amalgamation in the Embu Terrane, southern Ribeira Belt, Brazil. Lithos 342–343, 1–17. https://doi.org/10.1016/j.lithos.2019.05.024.
Patchett, P.J., Tatsumoto, M., 1980. Lu-Hf total-rock isochron for the eucrite meteorites. Nature 288, 571–574.
Peccerillo, A., Taylor, S.R., 1976. Geochemistry of eocene calc-alkaline volcanic rocks from the Kastamonu area, Northern Turkey. Contrib. Miner. Petrol. 58, 63–81. https://doi.org/10.1007/BF00384745.
Pedrosa-Soares, A.C., Vidal, P., Leonardos, O.H., Brito-Neves, B.B., 1998. Neoproterozoic oceanic remnants in eastern Brazil: further evidence and refutation of an exclusively ensialic evolution for the Aracuai-west Congo orogen. Geology 26, 519–522. https://doi.org/10.1130/0091-7613(1998)026<0519:NORIEB>2.3.CO;2.
Peixoto, E., Alkmim, F.F., Pedrosa-Soares, A.C., Lana, C., Chaves, A.O., 2018. Metamorphic record of collision and collapse in the Ediacaran-Cambrian Araçuaí orogen, SE-Brazil: insights from P-T pseudosections and monazite dating. J. Metamorph. Geol. 36, 147–172. https://doi.org/10.1111/jmg.12287.
Peixoto, C.D.A., Heilbron, M., Ragatky, D., Armstrong, R., Dantas, E.L., Valeriano, C.M., Simonetti, A., 2017. Tectonic evolution of the Juvenile Tonian Serra da Prata magmatic arc in the Ribeira belt, SE Brazil: implications for early west Gondwana amalgamation. Precambr. Res. 302, 221–254. https://doi.org/10.1016/j.precamres.2017.09.017.
Pe-Piper, G., Piper, D.J.W., Koukouvelas, I., Dolansky, L.M., Kokkalas, S., 2009. Postorogenic shoshonitic rocks and their origin by melting underplated basalts: the miocene of Limnos, Greece. Bull. Geol. Soc. Am. 121, 39–54. https://doi.org/10.1130/B26317.1.
Pimentel, M.M., 2016. The tectonic evolution of the Neoproterozoic Brasília Belt, central Brazil: a geochronological and isotopic approach. Braz. J. Geol. 46, 67–82. https://doi.org/10.1590/2317-4889201620150004.
Piuzana, D., Pimentel, M.M., Fuck, R.A., Armstrong, R., 2003. Neoproterozoic granulite facies metamorphism and coeval granitic magmatism in the Brasilia Belt, Central Brazil: regional implications of new SHRIMP U-Pb and Sm-Nd data. Precambr. Res. 125, 245–273. https://doi.org/10.1016/S0301-9268(03)00108-6.
Plank, T., 2005. Constraints from Thorium/Lanthanum on sediment recycling at subduction zones and the evolution of the continents. J. Petrol. 46, 921–944. https://doi.org/10.1093/petrology/egi005.
Profeta, L., Ducea, M.N., Chapman, J.B., Paterson, S.R., Gonzales, S.M.H., Kirsch, M., Petrescu, L., DeCelles, P.G., 2015. Quantifying crustal thickness over time in magmatic arcs. Sci. Rep. 5, 1–7. https://doi.org/10.1038/srep17786.
Putirka, K., Busby, C.J., 2007. The tectonic significance of high-K2O volcanism in the Sierra Nevada, California. Geology 35, 923–926. https://doi.org/10.1130/G23914A.1.
Pyle, J.M., Spear, F.S., Rudnick, R.L., McDonough, W.F., 2001. Monazite-xenotime-garnet equilibrium in metapelites and a new monazite-garnet thermometer. J. Petrol. 42, 2083–2107. https://doi.org/10.1093/petrology/42.11.2083.
Ragatky, C.D., 1998. Contribuição à geoquímica e geocronologia do Domínio São Roque e da Nappe de Empurrão Socorro-Guaxupé na região de Igaratá e Piracaia, SP. University of São Paulo.
Ramos, V.A., 2010. The tectonic regime along the Andes: present-day and Mesozoic regimes. Geol. J. 45, 2–25. https://doi.org/10.1002/gj.1193.
Reno, B.L., Brown, M., Kobayashi, K., Nakamura, E., Piccoli, P.M., Trouw, R.A.J., 2009. Eclogite-high-pressure granulite metamorphism records early collision in West Gondwana: new data from the Southern Brasília Belt, Brazil. J. Geol. Soc. 166, 1013–1032. https://doi.org/10.1144/0016-76492008-140.
Ribeiro, B.V., Faleiros, F.M., Campanha, G.A.C., Lagoeiro, L., Weinberg, R.F., Hunter, N.J.R., 2019. Kinematics, nature of deformation and tectonic setting of the Taxaquara Shear Zone, a major transpressional zone of the Ribeira Belt (SE Brazil). Tectonophysics 751, 83–108. https://doi.org/10.1016/j.tecto.2018.12.025.
Rocha, B.C., Moraes, R., Möller, A., Cioffi, C.R., Jercinovic, M.J., 2017. Timing of anatexis and melt crystallization in the Socorro-Guaxupé Nappe, SE Brazil: insights from trace

element composition of zircon, monazite and garnet coupled to U-Pb geochronology. Lithos 277, 337–355. https://doi.org/10.1016/j.lithos.2016.05.020.
Rocha, B.C., Moraes, R., Möller, A., Cioffi, C.R., 2018. Magmatic inheritance vs. UHT metamorphism: zircon petrochronology of granulites and petrogenesis of charnockitic leucosomes of the Socorro-Guaxupé nappe, SE Brazil. Lithos 314–315, 16–39. https://doi.org/10.1016/j.lithos.2018.05.014.
Rubatto, D., Hermann, J., Buick, I.S., 2006. Temperature and bulk composition control on the growth of monazite and zircon during low-pressure anatexis (Mount Stafford, Central Australia). J. Petrol. 47, 1973–1996. https://doi.org/10.1093/petrology/egl033.
Sato, K., Tassinari, C.C.G., Kawashita, K., Petronilho, L.A., 1995. O método geocronológico Sm-Nd no IG/USP e suas aplicações. Anais da Acad. Bras. Ciências.
Sato, K., Basei, M.A.S., Siga Jr., O., Sproesser, W.M., Passarelli, C.R., 2008. New techniques applied to the U-Pb Method at the centre for geochronological research of the university of sao paulo: chemical digestions, TIMS mass spectrometry and examples of integrated application of SHRIMP\rNovas tecnicas aplicadas ao metodo U-Pb no. Geologia USP - Serie Cientifica 8, 77–99.
Schmitt, R.S., Trouw, R.A.J., Van Schmus, W.R., Armstrong, R., Stanton, N.S.G., 2016. The tectonic significance of the Cabo Frio Tectonic Domain in the SE Brazilian margin: a Paleoproterozoic through Cretaceous saga of a reworked continental margin. Braz. J. Geol. 46, 37–66.
Segal, I., Halicz, L., Platzner, I.T., 2003. Accurate isotope ratio measurements of ytterbium by multiple collection inductively coupled plasma mass spectrometry applying erbium and hafnium in an improved double external normalization procedure. J. Anal. At. Spectrom. 18, 1217–1223. https://doi.org/10.1039/b307016f.
Shand, S.J., 1943. Eruptive Rocks: Their Genesis, Composition and Classification, with a Chapter on Meteorites, second ed. Wiley, New York.
Siivola, J., Schmid, R., 2007. List of Mineral abbreviations. IUGS Subcommission on the Systematics of Metamorphic Rocks pp. 1–14.
Silva, B.Y.B., 2017. Evolução Tectônica Da Porção Central Do Terreno Embu Ao Norte Da Zona De Cisalhamento Taxaquara-Guararema Terreno Embu Ao Norte Da Zona De Cisalhamento Taxaquara-Guararema.
Siqueira, R., Hollanda, M.H.B.M., Basei, M.A.S., 2014. A novel approach to (LA-ICP-MS acquired) U-Th-Pb data processing. South American Symposium on Isotope Geology. Instituto de Geociências, USP, São Paulo.
Söderlund, U., Patchett, P.J., Vervoort, J.D., Isachsen, C.E., 2004. The 176Lu decay constant determined by Lu-Hf and U-Pb isotope systematics of Precambrian mafic intrusions. Earth Planet. Sci. Lett. 219, 311–324. https://doi.org/10.1016/S0012-821X(04)00012-3.
Spear, F.S., Pyle, J.M., 2010. Theoretical modeling of monazite growth in a low-Ca metapelite. Chem. Geol. 273, 111–119. https://doi.org/10.1016/j.chemgeo.2010.02.016.
Spencer, C.J., Kirkland, C.L., Taylor, R.J.M., 2016. Geoscience Frontiers Strategies towards statistically robust interpretations of in situ U e Pb zircon geochronology. Geosci. Front. 7, 581–589. https://doi.org/10.1016/j.gsf.2015.11.006.
Stacey, J.S., Kramers, J.D., 1975. Approximation of terrestrial lead isotope evolution by a two-stage model. Earth Planet. Sci. Lett. 26, 207–221. https://doi.org/10.1016/0012-821X(75)90088-6.
Stern, R.J., 2002. Subduction zones. Rev. Geophys. 40. https://doi.org/10.1029/2001RG000108.
Stern, R.J., Bloomer, S.H., Lin, P.N., Ito, E., Morris, J., 1988. Shoshonitic magmas in nascent arcs: new evidence from submarine volcanoes in the northern Marianas. Geology 16, 426–430. https://doi.org/10.1130/0091-7613(1988)016<0426:SMINAN>2.3.CO;2.
Tang, M., Lee, C.T.A., Chen, K., Erdman, M., Costin, G., Jiang, H., 2019. Nb/Ta systematics in arc magma differentiation and the role of arclogites in continent formation. Nat. Commun. 10. https://doi.org/10.1038/s41467-018-08198-3.
Tassinari, C.C.G., 1988. As idades das rochas e dos eventos metamórficos da porção sudeste do Estado de São Paulo e sua evolução crustal. University of São Paulo.
Tassinari, C.C.G., Babinski, M., Nutman, A.P., 2004. A Idade e Natureza da Fonte do Granito do Moinho, Faixa Ribeira, Sudeste do Estado de São Paulo. Geologia USP - Série Científica 4, 91–100.
Tatsumi, Y., Eggins, S., 1995. Subduction Zone Magmatism, first ed. Blackwell Science.
Tedeschi, M., Novo, T., Pedrosa-Soares, A.C., Dussin, I., Tassinari, C.C.G., Silva, L.C., Gonçalves, L., Alkmim, F., Lana, C., Figueiredo, C., Dantas, E., Medeiros, S., Campos, C., Corrales, F., Heilbron, M., 2016. The Ediacaran Rio Doce magmatic arc revisited (Araçuaí-Ribeira orogenic system, SE Brazil). J. S. Am. Earth Sci. 68, 167–186. https://doi.org/10.1016/j.jsames.2015.11.011.
Tedeschi, M., Lanari, P., Rubatto, D., Pedrosa-Soares, A.C., Hermann, J., Dussin, I., Pinheiro, M.A.P., Bouvier, A.S., Baumgartner, L., 2017. Reconstruction of multiple P-T-t stages from retrogressed mafic rocks: subduction versus collision in the Southern Brasília orogen (SE Brazil). Lithos 294–295, 283–303. https://doi.org/10.1016/j.lithos.2017.09.025.
Tedeschi, M., Pedrosa-Soares, A.C., Dussin, I., Lanari, P., Novo, T., Pinheiro, M.A.P., Lana, C., Peters, D., 2018. Protracted zircon geochronological record of UHT garnet-free granulites in the Southern Brasília orogen (SE Brazil): petrochronological constraints on magmatism and metamorphism. Precambr. Res. 316, 103–126. https://doi.org/10.1016/j.precamres.2018.07.023.
Trouw, R.A.J., Heilbron, M., Ribeiro, A., Paciullo, F.V.P., Valeriano, C.M., Almeida, J.C. H., Tupinambá, M., Andreis, R.R., 2000. The Central Segment of the Ribeira Belt, in: Cordani, U.G., Milani, E.J., Thomaz Filho, A., Campos, D.A. (Eds.), Tectonic Evolution of South America. Rio de Janeiro, pp. 287–310. https://doi.org/10.4067/S0716-02082000000200006.
M. Tupinambá W. Teixeira M. Heilbron 2000. Neoproterozoic Western Gondwana Assembly and Subductionrelated Plutonism: the role of the Rio Negro Complex in the Ribeira Belt. Rev. Bras. Geociências 30, 007–011. 10.25249/0375-7536.2000301007011.
Turner, S., Arnaud, N., Liu, J., Rogers, N., Hawkesworth, C., Harris, N., Kelley, S., Van Calsteren, P., Deng, W., 1996. Post-collision, shoshonitic volcanism on the Tibetan plateau: implications for convective thinning of the lithosphere and the source of ocean island basalts. J. Petrol. 37, 45–71. https://doi.org/10.1093/petrology/37.1.45.
Valeriano, C.D.M., 2017. The Southern Brasília Belt. In: Heilbron, M., Cordani, U.G., Alkmim, F.F. (Eds.), São Francisco Craton. Springer International Publishing, Eastern Brazil, pp. 189–203. https://doi.org/10.1007/978-3-319-01715-0_10.
Valeriano, C.M., Mendes, J.C., Tupinambá, M., Bongiolo, E., Heilbron, M., Junho, M.C.B., 2016. Cambro-Ordovician post-collisional granites of the Ribeira belt, SE-Brazil: a case of terminal magmatism of a hot orogen. J. S. Am. Earth Sci. 68, 269–281. https://doi.org/10.1016/j.jsames.2015.12.014.
Van Schmus, W.R., Tassinari, C.C.G., Cordani, U.G., 1986. Estudo Geocronológico da parte inferior do Grupo São Roque. In: Congresso Brasileiro de Geologia. Goiânia, pp. 1399–1406.
Vermeesch, P., 2018. IsoplotR: a free and open toolbox for geochronology. Geosci. Front. 9, 1479–1493. https://doi.org/10.1016/j.gsf.2018.04.001.
Vinagre, R., Trouw, R.A.J., Mendes, J.C., Duffles, P., Peternel, R., Matos, G., 2014. New evidence of a magmatic arc in the southern Brasília Belt, Brazil: the Serra da Água Limpa batholith (Socorro-Guaxupé Nappe). J. S. Am. Earth Sci. 54, 120–139. https://doi.org/10.1016/j.jsames.2014.05.002.
Vinagre, R., Trouw, R.A.J., Mendes, J.C., Geraldes, M., Távora, A., Nepomuceno, F., Araújo Junior, E.B., 2017. Proterozoic evolution of part of the Embu Complex, eastern São Paulo state, SE Brazil. J. S. Am. Earth Sci. 79, 170–188. https://doi.org/10.1016/j.jsames.2017.08.003.
Vlach, S.R.F., 2008. Mineralogia, Análise e Datação de Monazita e Xenotima com Microssonda Eletrônica e Aplicações. Universidade de São Paulo.
Wang, Y., Foley, S.F., Prelević, D., 2017. Potassium-rich magmatism from a phlogopite-free source. Geology 45, 467–470. https://doi.org/10.1130/G38691.1.
Weaver, B.L., Tarney, J., 1984. Empirical approach to estimating the composition of the continental crust. Nature 310, 575–577. https://doi.org/10.1038/310575a0.
Westin, A., Campos Neto, M.C., 2013. Provenance and tectonic setting of the external nappe of the Southern Brasília Orogen. J. S. Am. Earth Sci. 48, 220–239. https://doi.org/10.1016/j.jsames.2013.08.006.
Westin, A., Campos Neto, M.C., Hawkesworth, C.J., Cawood, P.A., Dhuime, B., Delavault, H., 2016. A paleoproterozoic intra-arc basin associated with a juvenile source in the Southern Brasilia Orogen: application of U-Pb and Hf–Nd isotopic analyses to provenance studies of complex areas. Precambr. Res. 276, 178–193. https://doi.org/10.1016/j.precamres.2016.02.004.
Westin, A., Campos Neto, M.C., Cawood, P.A., Hawkesworth, C.J., Dhuime, B., Delavault, H., 2019. The Neoproterozoic southern passive margin of the São Francisco craton: insights on the pre-amalgamation of West Gondwana from U-Pb and Hf-Nd isotopes. Precambr. Res. 320, 454–471. https://doi.org/10.1016/j.precamres.2018.11.018.
Woodhead, J.D., Hergt, J.M., 2001. Strontium, neodymium and lead isotope analyses of NIST glass certified reference materials: SRM 610, 612, 614. Geostand. Geoanal. Res. 25, 261–266. https://doi.org/10.1111/j.1751-908X.2001.tb00601.x.